Lithos 344–345 (2019) 280–296

Contents lists available at ScienceDirect

Lithos

journal homepage: www.elsevier.com/locate/lithos

Across-arc geochemical variations in the Paleogene magmatic belt of Iran

Fatemeh Sepidbar [a,b,*], Hadi Shafaii Moghadam [a], Le Zhang [c], Jian-Wei Li [b], Jinlong Ma [c], Robert J. Stern [d], Chuan Lin [e]

[a] School of Earth Sciences, Damghan University, Damghan 36716-41167, Iran
[b] State Key Laboratory of Geological Processes and Mineral Resources, School of Earth Sciences, China University of Geoscience, Wuhan 430047, China
[c] State Key Laboratory of Isotope Geochemistry, Guangzhou Institute of Geochemistry, Chinese Academy of Sciences, Guangzhou 510640, PR China
[d] Geosciences Dept. University of Texas at Dallas, Richardson, TX 75083-0688, USA
[e] College of Oceanography, Hohai University, Nanjing 210093, PR China

ARTICLE INFO

Article history:
Received 26 April 2019
Received in revised form 18 June 2019
Accepted 20 June 2019
Available online 25 June 2019

Keywords:
Arc magmatism
Magmatic flare-up
Urumieh-Dokhtar Magmatic Belt
Iran

ABSTRACT

Across-arc geochemical variations between igneous rocks from the magmatic front (MF) to rear-arc (RA) are commonly observed for convergent margins, but the processes that are responsible for these variations are unclear. To address these questions, we studied a well-exposed Cenozoic continental arc, the Urumieh-Dokhtar Magmatic Belt (UDMB) of Iran and its rear-arc counterpart to the north.

North Iran RA magmatism is bimodal, characterized by mafic to felsic igneous rocks of calc-alkaline to shoshonitic affinity. The new zircon U -Pb ages show that plutonic rocks are ~ 42–38 Ma whereas volcanic rocks are older at ~52 Ma. $^{87}Sr/^{86}Sr_{(t)}$ and $\varepsilon Nd_{(t)}$ values of UDMB RA igneous rocks range from 0.70483 and 0.70783 and −2.5 and + 3.6, respectively. Zircons from plutonic rocks show εHf(t) values ranging from +1.8 to +9.8, higher than volcanic rocks with εHf (t) between +2.6 and −9.2. Isotopic data agrees with inferences from incompatible trace element ratios (*e.g.*, Th/Yb, Zr/Nb and La/Yb) that mafic plutonic rocks originated from an enriched mantle source, whereas felsic volcanic rocks show more interaction with continental crust. High magmatic fluxes did not occur at the same time in the MF and RA; UDMB MF flared-up at ~ 54–37 Ma and 20–5 Ma, overlapping RA magmatic flare-ups at 45–40 Ma and 30–25 Ma. The available major and trace element data from the UDMB show that most magmatic rocks experienced strong fractional crystallization and assimilation-fractional crystallization processes, making it difficult to identify across-arc geochemical variations. Moreover, the bulk rock εNd(t) and zircon εHf(t) values are highest at the MF, but the across-arc isotopic variability seems to be mainly controlled by crustal influence. High-flux magmatism in the UDMB was related to protracted heating of the crust as a result of subduction of Neotethys oceanic lithosphere. This weakened the continental lithosphere, leading to strong extension in Paleogene time accompanied by decompression melting and magmatic flare-ups.

1. Introduction

Iran has been a convergent plate margin for at least 90 million years, evolving from formation of a new subduction zone to a mature, extensional Andean-type arc in Paleogene time, culminating in collision with Arabia beginning in mid-Cenozoic time (Moghadam et al., 2018). Paleogene arc igneous rocks are common along the southern margin of Eurasia, from Turkey and the Caucasus eastward into Iran and into the Lhasa terrane of Tibet (*e.g.*, Chiu et al., 2013; Neill et al., 2013; Neill et al., 2015). The Paleogene magmatic flare-up of Iran was characterized by intense volcanism and plutonism along the Urumieh-Dokhtar Magmatic Belt (UDMB), which defined the magmatic front (MF), and also occurred behind it in the rear-arc (RA) to the north (the Alborz magmatic belt) and NE (Fig. 1).

The UDMB has been studied in greater detail due to Cu-Au mineralization in its central and southern sections. These studies have established that melting of the mantle wedge and perhaps the subducting slab were the primary sources of arc magmas, with minor assimilation of continental crust (Aghazadeh et al., 2011). Voluminous Cenozoic magmatism in Iran was stimulated by Eocene hyperextension and Neogene transtension (Verdel et al., 2011). Paleogene extension was also responsible for core complex formation in the Lut block (Saghand), between the magmatic front and the rear-arc (Kargaranbafghi et al., 2015). Geochronological data constrain the UDMB magmatic flare-up to *ca* 17 Myr episode in the Eocene, from ~54 Ma until 37 Ma, although there may have been a younger magmatic pulse at 20–5 Ma, mostly along the southern UDMB (Chiu et al., 2013; Verdel et al., 2007). Several causes are proposed for the Eocene flare-up, including decompression melting of lithospheric mantle hydrated

* Corresponding author at: School of Earth Sciences, Damghan University, Damghan 36716-41167, Iran
E-mail address: f.sepidbar@ut.ac.ir (F. Sepidbar).

https://doi.org/10.1016/j.lithos.2019.06.022
0024-4937/

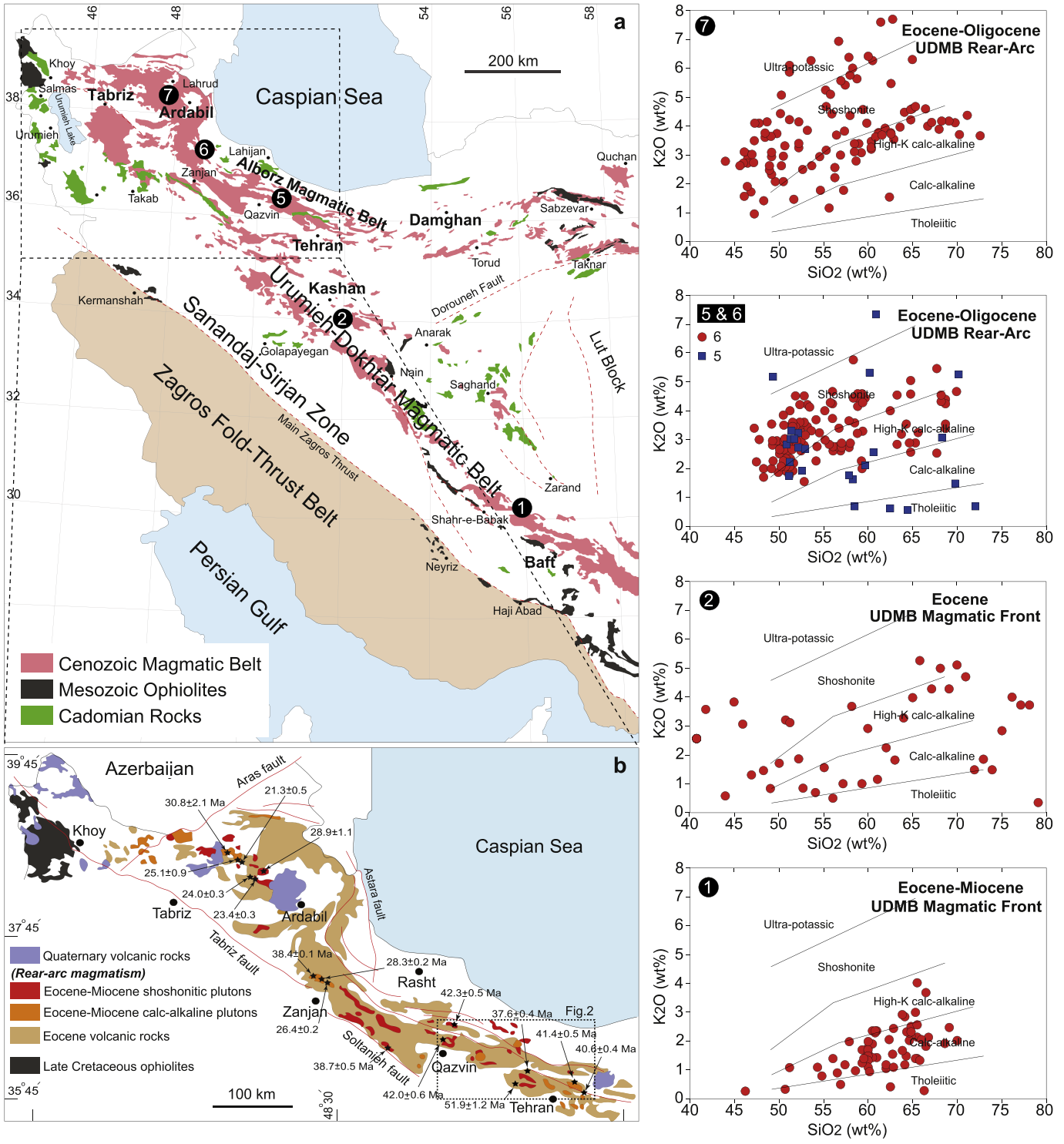

Fig. 1. (a) Map of Iran showing Cadomian basement rocks, Mesozoic ophiolites and Cenozoic igneous rocks. We have plotted rock samples from regions 1, 2 and 5–7 in a series of K_2O against SiO_2 diagrams to show the geochemical variations of the samples from UDMB magmatic front to rear-arc. The new data from this study (region 5) have been plotted as blue square (5). (b) Geological map showing the distribution of Eocene volcanic rocks, Eocene-Miocene calc-alkaline and shoshonitic intrusions and Quaternary volcanic rocks. Zircon U-Pb data are from ((Aghazadeh et al., 2011; Castro et al., 2013) and (Moghadam et al., 2017)). (For interpretation of the references to colour in this figure legend, the reader is referred to the web version of this article.)

by slab-derived fluids (Verdel et al., 2007),break-off of the Neotethyan slab and convective removal of thickened subcontinental lithospheric mantle (Pang et al., 2013). Despite the recognition of an Eocene flare-up in Iran (Verdel et al., 2007), how this was manifested in the MF *vs.* the RA is unclear.

Compared to our growing knowledge of the Paleogene UDMB, we understand far less about associated rear-arc magmatic rocks (Fig. 1). Two scenarios exist for Paleogene igneous rocks in N and NW Iran including: a) the development of a distinct northern arc relative to the UDMB (*e.g.*, Asiabanha and Foden, 2012); or b) the establishment of an associated rear-arc magmatic regime (Moghadam et al., 2018). Both hypotheses rely on insufficient geochemical, petrological and geochronological data. In fact, rear arc igneous activity is quite common at magmatically vigorous convergent margins, including the Andes,

Cascades, and NW Pacific (Jacques et al., 2014). Across-arc geochemical variations contain essential information about subduction zone magmatism and the associated processes. Mantle signatures of volcanic front lavas are often obscured by slab-derived components, but rear-arc magmatic rocks are less affected and often better reveal the composition of the mantle wedge (Jacques et al., 2013; Wehrmann et al., 2014).

In this study, we present the first systematic geochemical, isotopic and geochronological (zircon U-Pb) study of Paleogene Iran rear-arc igneous rocks. The primary goals of this paper are: 1) to establish the timing of rear-arc magmatism in N Iran using our new zircon U-Pb age results; 2) to characterise, based on their petrology and geochemistry, the source and origin of Paleogene rear-arc magmatism in N Iran; and 3) to reveal Paleogene across-arc geochemical variations between the UDMB magmatic front and rear-arc.

2. Geological background

The Urumieh-Dokhtar Magmatic Belt is 50–80 km wide, defines the magmatic front of the Cenozoic Iran arc and trends NW-SE for 1000 km across Iran between 28° and 39°N (Fig. 1A). This magmatic belt includes a thick (~4 km) pile of early calc-alkaline and late shoshonitic as well as adakitic rocks. The UDMB also contains several large Plio-Quaternary stratovolcanoes (Allen et al., 2013).

Several rear-arc basins developed NW and NE of the UDMB during the latest Cretaceous to Eocene, where marine and subaerial sediments were deposited associated with volcanic rocks, including thick sequences of marine pyroclastic rocks such as the Karaj Formation (Fig. 2; (Verdel et al., 2011). Voluminous magmatism produced up to ~3000 m-thick volcanic and pyroclastic sequences and edifices along with sedimentary intercalations. Rear-arc magmatism differs between NE and N Iran; NE Iran RA activity was mostly subaerial whereas N RA activity was mostly submarine with thick sequences of pyroclastic rocks and clastic sediments. Intrusive bodies ranging in composition from gabbro to granite are also common.

Paleogene arc magmatism across the Iran arc - both along the magmatic front and in the rear-arc - was remarkably heterogeneous in composition and petrological characteristics. Igneous and pyroclastic rocks of intermediate to acidic composition dominate along the MF, with few mafic rocks. In contrast, mafic rocks are more abundant in the RA. Shoshonitic rocks are mostly restricted to the RA regions (Fig. 1) (Asiabanha and Foden, 2012; Castro et al., 2013; Moghadam et al., 2018).

Paleogene rear-arc igneous activity developed partly in response to the thinning of Iran continental crust associated with extension. Several transgressive-regressive cycles are recorded in Iran RA sediments during latest Cretaceous to Eocene (Ballato et al., 2011). Mid- to late Paleocene regression led to emergence and deposition of red volcano-sedimentary sequences. These units in NE Iran consist of clastic sediments that grade from sandstones to conglomerates, with intercalated mafic to andesitic lavas, and minor interbedded intermediate to felsic pyroclastic rocks. In N Iran, pyroclastic rocks dominate over clastic sediments (Verdel et al., 2007). A marine transgression beginning in early to middle Eocene time is represented by thick (500–1000 m) sequences of deep marine Nummulitic limestones in NW and NE Iran. These limestones vary in thickness and often grade into fine-grained pyroclastic rocks. Eocene flare-up magmatism in both the FA and RA of Iran coincides with Eocene transgressions, which occurred during a time of rapidly falling sea-level globally (Miller et al., 2005), suggesting that magmatism was associated with subsidence related to extension. Eocene intermediate-mafic (calc-alkaline and OIB-like) intrusive rocks and extensional basins are also abundant along the Sanandaj-Sirjan Zone (SaSZ) of Iran (Fig. 1, in the outboard parts of the UDMB) (Deevsalar et al., 2017; Zhang et al., 2018). The occurrence of Eocene magmatic rocks in the SaSZ is ascribed to mantle melting due to break-off of the subducted Neotethyan oceanic slab (Deevsalar et al., 2017).

Cenozoic rear-arc magmatism in N Iran was built on Ediacaran-Early Paleozoic (Cadomian) crystalline basement. This basement is exposed NW of Karaj (Fig. 2) and can be traced NW-ward into Ediacaran rocks of Lahijan and Zanjan (Fig. 1A). NW of Karaj, Ediacaran volcano-sedimentary rocks (the Kahar Formation) including glacial sediments, are found (Etemad-Saeed et al., 2015). Ediacaran sediments are overlain

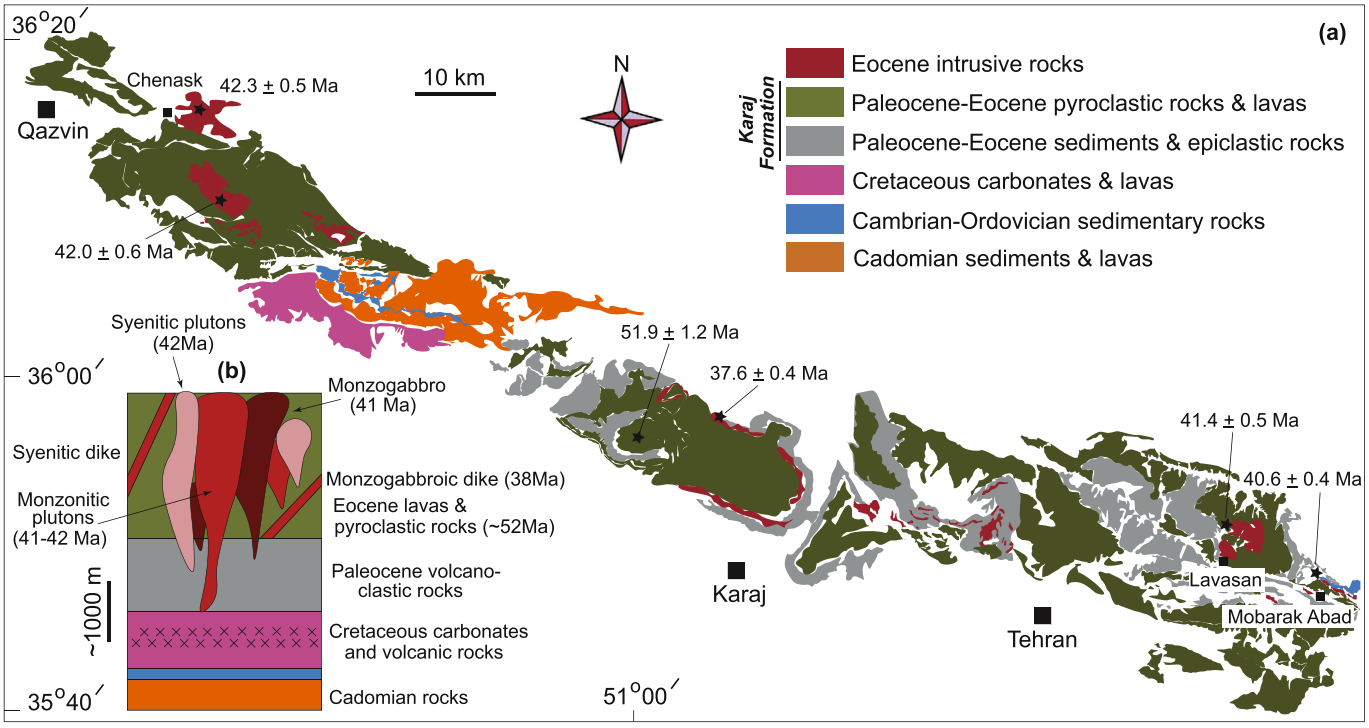

Fig. 2. (a) Simplified geological map of the studied area in N Iran (modified after Tehran, Karaj and Qazvin 1/250000 maps, Geological Survey of Iran). (b) Simplified stratigraphic column showing the rock relationships in N Iran rear-arc.

stratigraphically by Cambrian-Ordovician clastic sediments and by Cretaceous carbonates and basaltic-andesitic rocks (Fig. 2). Mesozoic volcano-sedimentary rocks are unconformably covered by Paleocene to Eocene volcanic rocks and pyroclastic deposits. Paleogene volcanic rocks mainly consist of andesites and basalt with less abundant acidic rocks. Andesitic pyroclastic rocks (the Karaj Formation) are abundant.

There are several mafic to acidic intrusions into Cenozoic volcano-sedimentary rocks in N and NW Iran with U-Pb zircon ages of ~21–39 Ma (Castro et al., 2013; Moghadam et al., 2017) (Fig. 1B). These intrusions and associated volcanic rocks show shoshonitic and high-K calc-alkaline geochemical signatures (Asiabanha and Foden, 2012; Castro et al., 2013). (Asiabanha and Foden, 2012) proposed a post-collisional setting for shoshonitic intrusions near Zanjan, whereas (Castro et al., 2013) proposed extension and melting of a metasomatized mantle source for similar intrusions near Lahrud (Fig. 1). Both bulk rock Nd and zircon Hf isotope data indicate that mantle-derived (juvenile) magmas interacted with Cadomian crust to generate these granitoid magmas (Moghadam et al., 2017).

There are also numerous undated mafic to acidic intrusions in N Iran. The main intrusions are Mobarak-Abad and Lavasan NE of Tehran, the Karaj intrusion north of Karaj and those east of Qazvin (Fig. 2). A biotite $^{40}Ar/^{39}Ar$ age of 37.2 ± 0.38 Ma is reported for the Mobarak-Abad gabbros (Verdel et al., 2011). There are few geochronologic data for the host rocks of these intrusions. Zircon U-Pb ages from andesites and tuffs north of Karaj (from the base and top of the Karaj Formation) are 47.4 ± 3.8 Ma and 36.0 ± 0.2 Ma respectively (Ballato et al., 2011). (Verdel et al., 2011) also reported zircon U-Pb ages of 49.3 ± 2.9 Ma, 45.3 ± 2.3 Ma, and 41.1 ± 1 for the Karaj tuffs.

Based on the available age information, RA magmatism in N Iran was active for ~15 Myr, from ~49 to 36 Ma (early to late Eocene). To further examine the timing of the RA magmatism, we report here new zircon U-Pb zircon ages for igneous rocks from N Iran. Geochemical and isotopic data are also reported and used to reconstruct the geochemical evolution of Eocene rear-arc magmatism and contrast this with better known coeval UDMB igneous rocks.

3. Field geology and petrography

We collected representative samples from plutonic and volcanic rocks from NE of Tehran to Qazvin (Fig. 1A). Our RA samples come from the Mobarak-Abad and Lavasan intrusions NE of Tehran and Karaj intrusive rocks from N of Karaj and Chenask intrusions E of Qazvin. We also collected associated volcanic rocks around the intrusions for geochronological and geochemical analyses. Below we discuss these rocks in more detail.

3.1. Mobarak-Abad intrusion

The Mobarak-Abad (MA) intrusion occupies an area of ~ 5 km^2. This intrusion is dominated by monzogabbro and occurs as an elongated body bounded by NW-SE trending faults (Fig. 2). The intrusive contact of this monzogabbro with Eocene volcanic and pyroclastic rocks is obvious in its southern parts, whereas in the north, the gabbro abuts Cambrian-Ordovician sedimentary rocks.

MA gabbros have medium-grained granular texture. The main minerals are euhedral to subhedral phenocrysts of plagioclase (~45 vol%), alkali feldspar (~15%), pyroxene (~25%), olivine (~5%), amphibole and biotite (~5%) and quartz (<2%). Magnetite, apatite and ilmenite are accessory minerals (< 3%). Subhedral to anhedral plagioclase (0.5–2 mm) are altered to kaolinite and sericite (Fig. S2A). Plagioclase are zoned, with compositions between andesine and labradorite. Rare quartz grains are interstitial between plagioclase and alkali feldspar. Clinopyroxenes contain inclusions of magnetite, amphibole and biotite. They are uralitized and partly replaced by chlorite. In the quartz-alkali feldspar-plagioclase (QAP) diagram (Streckeisen, 1979), MA intrusive rocks show monzogabbroic compositions (Fig. 3A).

3.2. Lavasan intrusion

The Lavasan intrusion occupies an area of ~35 km^2. It has intrusive contacts with Paleocene-Eocene volcanic rocks including andesites, basalts and pyroclastic rocks (Figs. 2, S1A-B). The Lavasan stock is a composite intrusion composed of syenite and monzonite (Fig. 3A). Monzonite occurs in the centre of the stock whereas syenite is exposed near the northern and southern margins. Syenites are pinkish and porphyritic and are characterized by abundant subhedral to anhedral orthoclase and minor sodic plagioclase, amphibole, biotite, quartz (<5%) and rare pyroxene (Fig. S2B). Zircon, apatite, titanite and opaque minerals are accessories. Alkali feldspars contain small inclusions of euhedral plagioclase and subhedral biotite. Plagioclase is partly altered to sericite and carbonate. Rare clinopyroxene occurs as fine-grained interstitial crystals between feldspars and as inclusions in feldspar. Subhedral to anhedral amphiboles occur as fine- to medium-grained phenocrysts. Anhedral quartz is interstitial between feldspars.

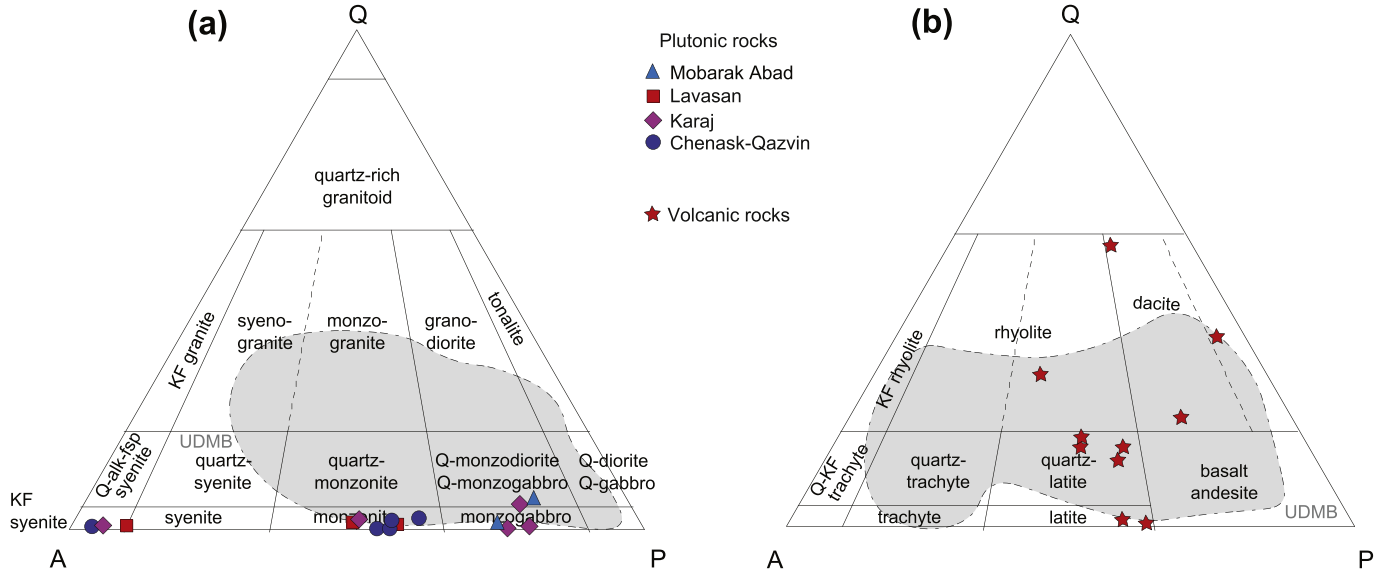

Fig. 3. A- Quartz-alkali feldspar-plagioclase (QAP) (Streckeisen, 1979) diagram for the classification of the N Iran plutonic (a) and volcanic (b) rocks. Data on Urumieh-Dokhtar Magmatic Belt (UDMB) are from (Honarmand et al., 2013) and Moghadam et al., (*unpublished data*).

Monzonites are coarse-grained and contain plagioclase, quartz, amphibole, biotite, and minor alkali feldspar (Fig. Fig. S2C). Subhedral to euhedral plagioclase is the major mineral. Plagioclase is lath-shaped and zoned, with compositions between oligoclase and labradorite. Orthoclase is interstitial between plagioclase and also rims plagioclase. Anhedral quartz occurs as small inclusions within feldspar and amphibole. Amphibole is partly replaced by chlorite and minor epidote and biotite is common.

3.3. Karaj intrusive rocks

Karaj intrusive rocks occur as ring sills and dikes injected into Paleocene-Eocene strata including tuffs and lavas of the Karaj Formation (Figs. 2, S1C). Karaj intrusive rocks are mainly monzogabbros, monzonites and rare syenites (Fig. 3A). Monzogabbros, the dominant lithology, contain plagioclase and clinopyroxene as the main minerals whereas olivine, apatite, biotite and titanomagnetite are accessories. Monzonites contain more plagioclase (Fig. S2D) and amphibole with minor K-feldspar whereas syenites contain more alkali feldspar and less amphibole. Plagioclase is usually altered to sericite, epidote, calcite, and titanite, especially their cores (Fig. S2D). Clinopyroxenes are occasionally uralitized and replaced by chlorite.

3.4. Chenask (E Qazvin) intrusion

The Chenask intrusion occupies ~100 km^2 and intrudes Eocene volcanic rocks, green tuffs, crystal lithic tuffs, tuffites, calcareous tuffs, marls and minor arkosic sandstones and volcanic wackes (Fig. S1D). Monzonites are the most common lithology, while syenites are rare (Fig. 3A).

Monzonites consist of plagioclase, alkali feldspar, amphibole, biotite and minor clinopyroxene (Fig. S2E). Plagioclase is subhedral to anhedral and ranges in size from 0.2 to 3 mm. Alkali feldspar laths vary from 0.5 to 2.5 mm. Biotite and amphibole show slight alteration into chlorite. Syenites consist predominantly of alkali feldspar and amphibole along with minor plagioclase, quartz and biotite. Both alkali feldspar and plagioclase are altered into sericite and titanite and amphiboles are chloritized. Zircon, apatite and opaque minerals occur as accessories.

3.5. Volcanic rocks (the Karaj Formation)

Paleocene-Eocene volcano-sedimentary rocks include dominant pyroclastic rocks and subordinate lava flows associated with Paleocene-Eocene submarine sedimentary rocks, making the ~3000 m thick Karaj Formation. These rocks are widespread in N Iran and are the main host of Paleogene intrusive rocks. These rocks were deposited in a subsiding marine basin.

The volcanic rocks vary from rhyolite-dacite to latite and quartz latite (Fig. 3B). Dacites and rhyolites are porphyritic with phenocrysts of plagioclase, alkali feldspar (sanidine), biotite and resorbed quartz in a glassy matrix (Fig. S2F). Sanidine is present as randomly oriented, tabular crystals in dacites whereas in rhyolites, they are occasionally oriented. Sanidine in some dacitic lavas is altered into sericite and carbonate (Fig. S2F). Latites generally accompany dacites and contain more plagioclase than sanidine along with more mafic minerals such as zoned clinopyroxene and amphibole (Fig. S2G). Iddingsitized olivines are common in some latites (Fig. S2G). Apatite and iron oxides (magnetite and titanomagnetite) are also present. These rocks are more crystalline than are dacites and rhyolites.

4. Analytical procedures

We used five main analytical procedures including: 1) X-Ray Fluorescence (XRF) and Inductively Coupled Plasma-Mass Spectrometry (ICP-MS) for whole-rock major- and trace-element analyses; 2) Cathodoluminescence imaging of zircons; 3) Laser Ablation-Inductively Coupled Plasma-Mass Spectrometry (LA-ICPMS) analyses for U-Pb zircon ages; 4) Multi-Collector Inductively Coupled Plasma-Mass Spectrometry (MC-ICP-MS) to analyse zircon Lu-Hf isotopes; and 5) Thermal ionization mass spectrometry for Sr and Nd isotopes in whole-rock samples. We studied >70 samples petrographically, 25 for whole-rock chemical analysis, 6 for LA-ICPMS U-Pb zircon ages, 6 for Lu-Hf analysis and 10 for Sr-Nd isotopes. We selected fresh samples for whole rock geochemistry. Analytical details are presented in Appendix A.

5. Results

5.1. Major- and trace-element geochemistry

We analysed 16 plutonic rock samples and 10 volcanic rock samples. Major, trace and REE data are given in Table S1.

In the total alkalis *vs* silica diagram (Middlemost, 1994), the RA plutonic rocks have high alkali contents and plot in syenite, monzonite, monzodiorite and gabbro fields (Fig. 4A). Volcanic rocks also have different compositions and fall in the fields of trachybasalt to rhyolite (Fig. 4B). Monzogabbros are characterized by rather constant SiO_2 (49.8–52.6 wt%) but with high Al_2O_3 (16.9–21.2 wt%) and K_2O (1.9–2.9 wt%). Monzonites have a wide range of SiO_2 (50.2–59.6 wt %), Al_2O_3 (16.7–21.5 wt%) and K_2O (0.6–5.2 wt%). Syenites have higher contents of SiO_2 (60.5–64.2 wt%), but variable K_2O values (0.5–7.2 wt%). In the Al_2O_3/ ($CaO + K_2O + Na_2O$), *i.e.* A/CNK, *vs* SiO_2 diagram (Chappell, 1999), these rocks show metaluminous to slightly peraluminous affinities (Fig. 4C). In the K_2O-SiO_2 (Fig. 4D) and Th-Co (Fig. 4E) co-variation diagrams, most plutonic and volcanic rocks have calc-alkaline to shoshonitic signatures, although some samples have low contents of K_2O (Fig. 4D & E). Both volcanic and plutonic rocks are characterized by variable Sr (44.5–885 ppm), with low Y (13.3–41.7 ppm) and Yb (1.5–4.4 ppm) contents. The Sr/Y ratio (1.5–44.9) of the N Iran RA igneous rocks correspond to normal arc rocks (Fig. 4F).

North Iran RA plutonic and volcanic rocks show similar rare earth and trace element patterns in chondrite- and N-MORB-normalized diagrams (Fig. 5). Chondrite-normalized rare earth element (REE) patterns for both plutonic and volcanic rocks are enriched in light REEs (LREEs) compared to heavy REEs (HREEs) (*e.g.*, $La_{(n)}/Yb_{(n)} =$ 2.04–12.70), without conspicuous negative Eu anomalies ($Eu/Eu^* =$ 0.61–1.02) (Fig. 5). In an N-MORB-normalized multi-element diagram, enrichment in Rb, Ba, Th, U and K, and modest negative anomalies in high field strength elements (HFSEs) such as Nb, Ti and P, are noticeable for the N Iran RA igneous rocks (Fig. 5). These rocks are weakly fractionated in HREEs compared to MREEs ($Gd_{(n)}/Yb_{(n)} = 1.73–2.18$) (Fig. 5) and show control by feldspar, not garnet. Geochemically, the rare earth and trace element patterns of N Iran RA magmatic rocks are similar to shoshonitic rocks. Similar high-K calc-alkaline and shoshonitic volcanic rocks are also reported from near Qazvin (Asiabanha and Foden, 2012).

5.2. Bulk rock Sr-Nd isotope

Nd-Sr isotopic ratios of plutonic and volcanic rocks from N Iran RA are given in Table S2. The $^{87}Sr/^{86}Sr_{(t)}$ and $^{143}Nd/^{144}Nd_{(t)}$ ratios were calculated using an age of 40 Ma. The $^{87}Sr/^{86}Sr_{(t)}$ and $\varepsilon Nd_{(t)}$ values of the RA igneous rocks span a range of 0.70483 and 0.70783 and − 2.5 and + 3.6, respectively. The isotopic composition of the plutonic rocks lies within the upper right quadrant of the Sr-Nd isotope diagram (Fig. 6A), except for two volcanic samples which fall within the enriched (lower right) quadrant (Fig. 6A). Some igneous rocks have radiogenic Nd but less radiogenic Sr, whereas three monzonites and monzogabbros have higher (>0.706) $^{87}Sr/^{86}Sr_{(t)}$ and are close to the isotopic values of the EMII mantle source. Volcanic rocks with less radiogenic Nd probably show more contamination with the Late

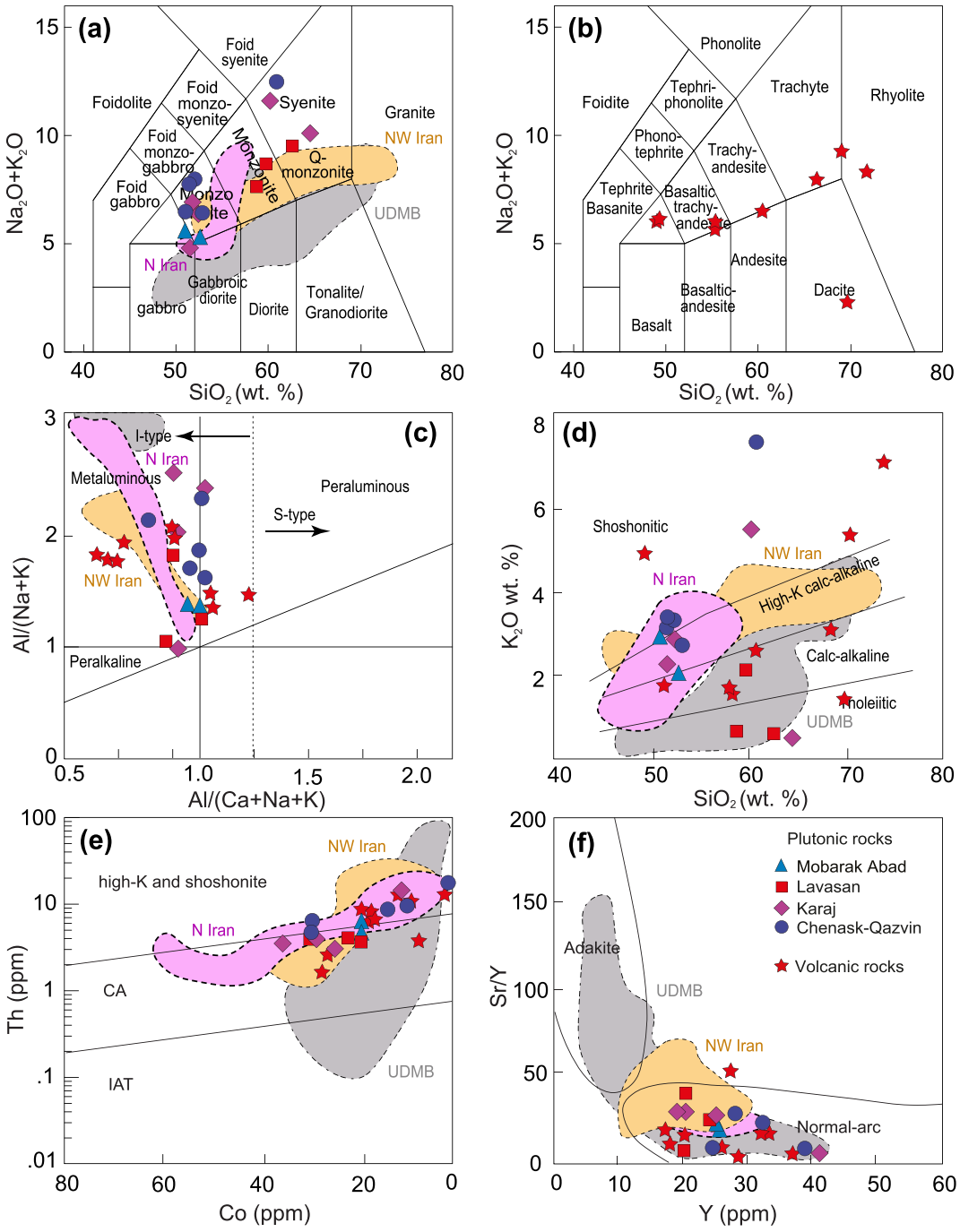

Fig. 4. Plots of $Na_2O + K_2O$ for classifying plutonic (a) and volcanic (b) rocks from N Iran (modified after (Lebas et al., 1986)). Alumina saturation index (c) and K_2O *vs* SiO_2 (d) for N Iran RA magmatic rocks. Th *vs* Co (Hastie et al., 2007) (e) and Sr/Y *vs* Y (f) diagrams for discriminating magmatic rocks from N Iran rear-arc (the fields for adakite and normal island-arc dacites and rhyolites are based on the work of (Castillo, 2012; Defant and Drummond, 1990)). Data for NW and N Iran magmatic rocks are from (Aghazadeh et al., 2011; Asiabanha and Foden, 2012; Castro et al., 2013) and (Moghadam et al., 2017). Data on Urumieh-Dokhtar Magmatic Belt (UDMB) are from (Honarmand et al., 2013) and Moghadam et al., (*unpublished data*).

Neoproterozoic continental crust of Iran. All samples plot between a MORB-type depleted mantle and Cadomian continental crust; gabbros have more radiogenic Nd *versus* volcanic rocks with less radiogenic Nd. Our rocks have low $^{147}Sm/^{144}Nd$ ratios ranging from 0.1363 to 0.0894, except dacites with higher $^{147}Sm/^{144}Nd > 0.1496$. A two-stage Nd isotopic model ages (T_{DM}) of N Iran samples range from 0.3 to 0.7 Ga for intrusive rocks and 1.2 Ga for volcanic rocks. A two-stage mantle model age is better for the rocks with evidence of crustal contamination. In this case it is assumed that a significant change in Sm/Nd ratio occurred during fractionation and/or mixing in the crust, after extraction from the mantle.

5.3. Zircon U-Pb geochronology

We analysed 6 samples for zircon U-Pb ages including monzogabbro (2 samples), monzonite (2 sample), syenite (1 sample) and dacite (1 sample). CL images and U-Pb age results are shown in Figs. 7 and 8 and are given in Table S3.

5.3.1. Sample A-2-1 (Mobarak Abad monzogabbro)

Sixteen zircon grains from the Mobarak Abad monzogabbro were dated by LA-ICPMS. Cathodoluminescence (CL) images

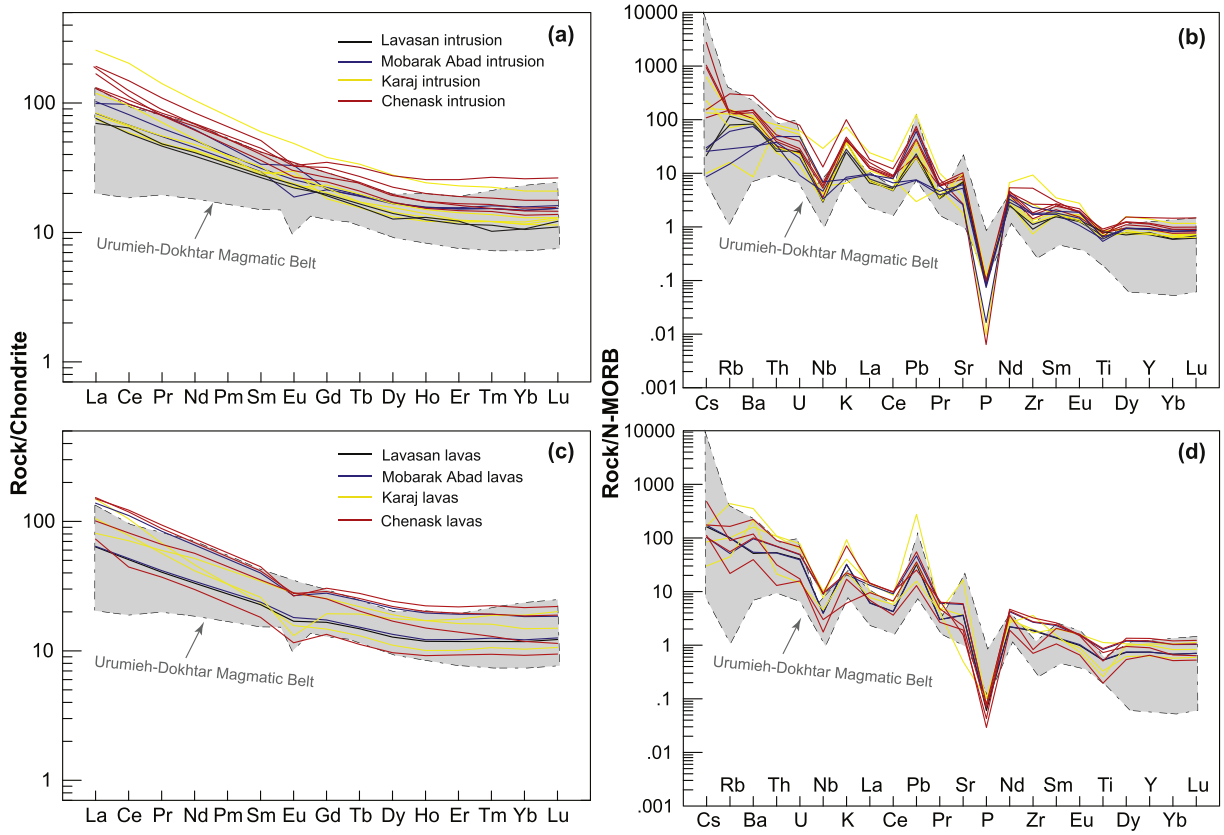

Fig. 5. Chondrite- and N-MORB-normalized REE and trace-element patterns of the N Iran igneous rocks. Normalization data are from (Sun and McDonough, 1989). Data on Urumieh-Dokhtar Magmatic Belt (UDMB) are from (Honarmand et al., 2013) and Moghadam et al., (*unpublished data*).

show that zircons are long prismatic and mostly are euhedral to subhedral (Fig. 7A). Zircons are ~100–250 μm long, with length to width ratios of 2:1 to 1:1. Zircons show oscillatory zoning in CL images (Fig. 7A) confirming a magmatic origin (Belousova et al., 2002). Analysed zircons show a weighted mean $^{206}Pb/^{238}U$ age of 40.6 ± 0.4 Ma (MSWD = 1.4) (Fig. 8A). Older zircons are also present and are interpreted both as earlier components in a long-lived magma chamber ($^{206}Pb/^{238}U$ ages of 45–46 Ma) and inherited zircons from older continental crust ($^{206}Pb/^{238}U$ age of 123.4 Ma).

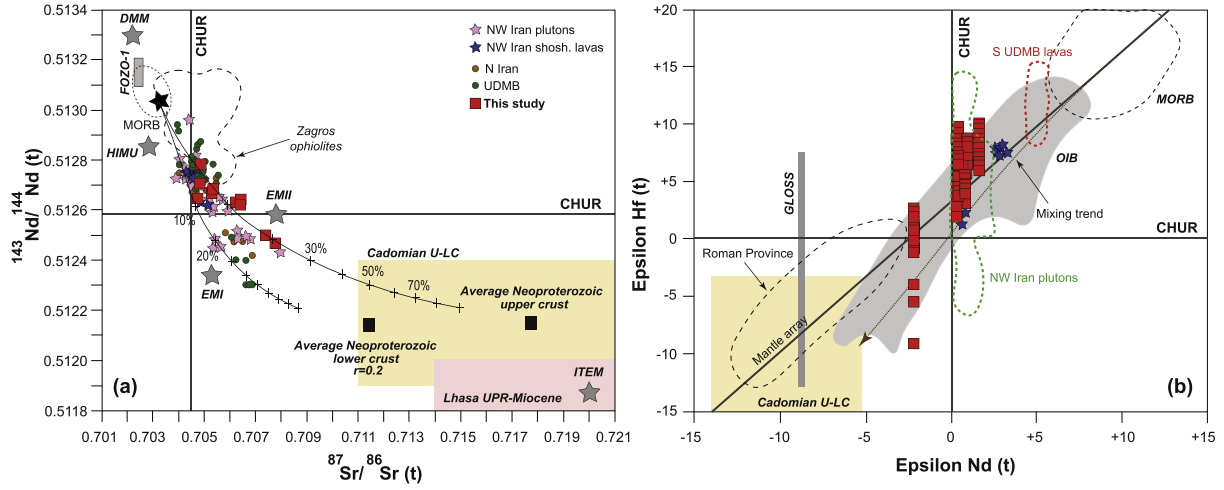

Fig. 6. $^{143}Nd/^{144}Nd$ *vs* $^{87}Sr/^{86}Sr$ (a) for the N Iran RA rocks compared with the mantle components HIMU, EMI, EMII, DMM (Zindler and Hart, 1986); FOZO1 (Hart and Hauri, 1992), ITEM (Bell et al., 2004); and CHUR (Chondritic Uniform Reservoir). Data for the Cadomian upper and lower crust (U-LC) rocks are from (Moghadam et al., 2015). Data for Lhasa ultrapotassic rocks (UPR) are from (Wang et al., 2014). Isotope data for NW and N Iran magmatic rocks are from (Aghazadeh et al., 2011; Asiabanha and Foden, 2012; Castro et al., 2013) and (Moghadam et al., 2017). Data on Urumieh-Dokhtar Magmatic Belt (UDMB) are from (Honarmand et al., 2013) and Moghadam et al., (*unpublished data*). The AFC modelling is according to formula presented by (Ersoy and Palmer, 2013). The composition of the starting melt is similar to island-arc tholeiitic lavas from NE Iran and Zagros ophiolites. The composition of average Cadomian lower and upper crust is according to (Moghadam et al., 2015). We assume that the main assimilant of Cenozoic Iran arc magmas was Late Neoproterozoic (Cadomian) crust, as these outcrop widely in Iran and there are abundant Cadomian inherited and xenocrystic zircons in most Cenozoic Iran arc magmatic rocks. b- εHf(t) *vs* εNd(t) for the N Iran RA magmatic rocks. MORB and OIB data are from (Chauvel and Blichert-Toft, 2001; Pearce et al., 1999). Mantle array data are after (Vervoort and Blichert-Toft, 1999).

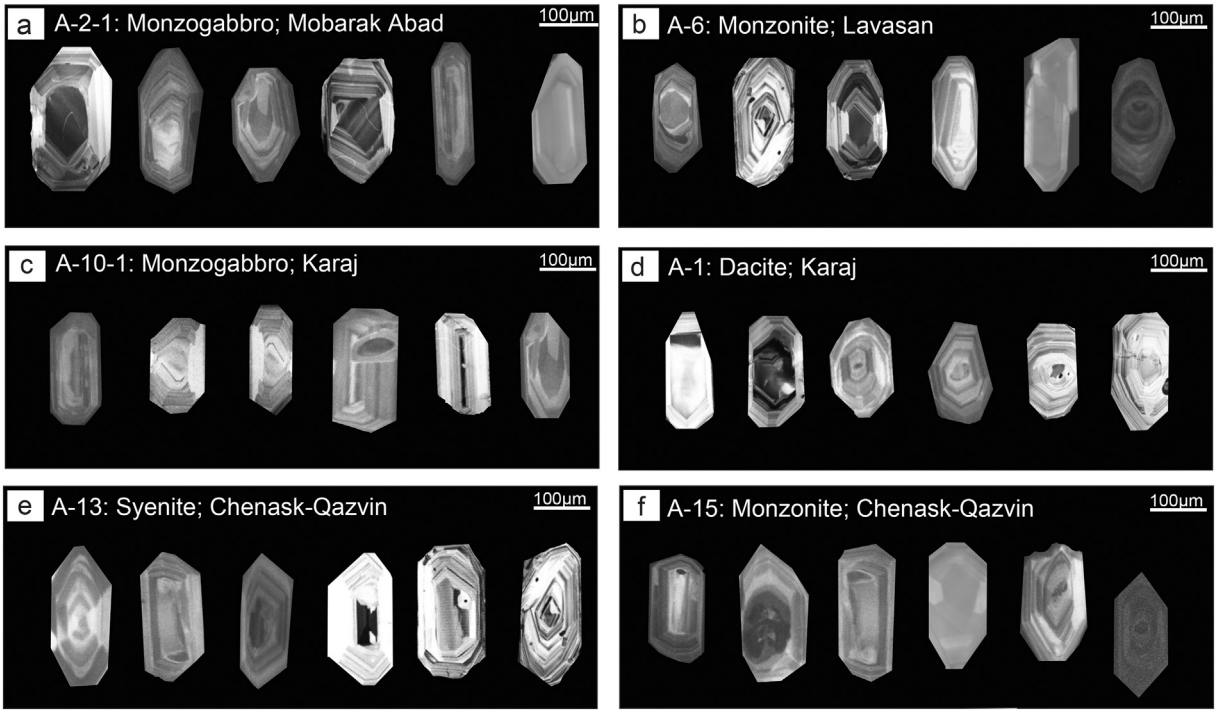

Fig. 7. Cathodoluminescence images of the dated samples from the N Iran rear-arc.

5.3.2. Sample A-6 (Lavasan monzonite)

Zircons from the Lavasan intrusion are long prismatic (> 150 μm) with length to width ratios of 2:1 to 1:1. Zircons show oscillatory zoning, although some are unzoned. Inherited cores are distinguished in the CL images. The analysed zircons reveal a weighted mean $^{206}Pb/^{238}U$ age of 41.4 ± 0.5 Ma (MSWD = 1.8) (Fig. 8B). Some zircons are slightly older with $^{206}Pb/^{238}U$ ages of 42 to 45 Ma. These zircons may represent an earlier component that crystallized in the magma chamber, suggesting slow cooling (Schaltegger et al., 1999).

5.3.3. Sample A-10-1 (Karaj monzogabbro)

This sample is from the Karaj sill-like gabbroic intrusion. Zircons are 100 to 200 μm long, with length to width ratios between 1:1 and 2:1. Most zircons are euhedral and exhibit oscillatory zoning (Fig. 7C). Fourteen analysed grains cluster with a weighted mean $^{206}Pb/^{238}U$ age of 37.6 ± 0.4 Ma (MSWD = 0.6) (Fig. 8C).

5.3.4. Sample A-1 (Karaj dacite)

This sample comes from felsic lavas interlayered with the Karaj Formation pyroclastic rocks. Zircons are 100 to 200 μm long, with length to width ratios between 1:1 and 2:1. Zircons are mostly euhedral and exhibit oscillatory zoning (Fig. 7D). Fifteen analysed zircons yield a weighted mean $^{206}Pb/^{238}U$ age of 51.9 ± 1.2 Ma (MSWD = 2.3) (Fig. 8D). CL images reveal some inherited cores, with $^{206}Pb/^{238}U$ ages of 63–99, 240 and 408–424 Ma.

5.3.5. Sample A-15 (Chenask monzonite)

This sample comes from the mafic parts of the Chenask (E Qazvin) intrusion. Zircons are euhedral to subhedral (Fig. 7F) with lengths of ~100–250 μm and length to width ratios of 2:1 to 1:1. Zircons show weak oscillatory zoning in CL images and some are unzoned (Fig. 7F). A total of 30 analyses define a weighted mean $^{206}Pb/^{238}U$ age of 42.3 ± 0.5 Ma (MSWD = 0.6) (Fig. 8F).

5.3.6. Sample A-13 (Chenask syenite)

This sample is from the felsic parts of the Chenask (E Qazvin) intrusion. We analysed twenty zircon grains from this sample. CL images reveal zircons with well- to weakly developed oscillatory zoning (Fig. 7E). Zircons cluster with a weighted mean $^{206}Pb/^{238}U$ age of 42.0 ± 0.6 Ma (MSWD = 1.8) (Fig. 8E).

5.4. Zircon Hf isotopes

Measured $^{176}Lu/^{177}Hf$ and $^{176}Hf/^{177}Hf$ ratios of zircons in N Iran RA magmatic rocks are summarised in Table S3. Zircons from monzogabbros (samples A-2-1 and A-10-1) show εHf(t) values ranging from +4.2 to +9.8 (Table S3). Two-stage model ages (T^C_{DM}) for monzogabbro zircons using a $^{176}Lu/^{177}Hf$ value of 0.015 (Griffin et al., 2004) show young ages (480–850 Ma), confirming the juvenile nature of the monzogabbroic magmas. Monzonites (samples A-15 and A-6) have zircons with slightly lower εHf(t) values; +1.8 to +8.7 and T^C_{DM} between 580 and 1000 Ma. Syenite (sample A-13) also has positive εHf (t) values between ~ + 3 and + 7, with T^C_{DM} = 670–930 Ma. Dacite (A-1) magmatic zircons have εHf (t) between +2.6 and − 9.2, with T^C_{DM} = 0.9 to 1.7 Ga. The inherited zircons have even more variable εHf (t) values; +4.1 to −20.2 with T^C_{DM} = 1–2.4 Ga. On a zircon εHf (t) *vs* bulk rock εNd (t) plot, plutonic rocks appear to have originated from enriched mantle, similar to that responsible for OIBs, whereas volcanic rocks have less radiogenic Nd and Hf and plot toward the Cadomian crust of Iran (Fig. 6B).

6. Discussion

Here we use our new results to discuss 6 topics: 1) source of N Iran igneous rocks; 2) Lu-Hf isotopic systematics; 3) ages of RA *vs* MF rocks; 4) across-arc geochemical variations; 5) fractional crystallization and assimilation-fractional crystallization processes in Iran arcs; and 6) hyperextension and arc magmatism in Iran.

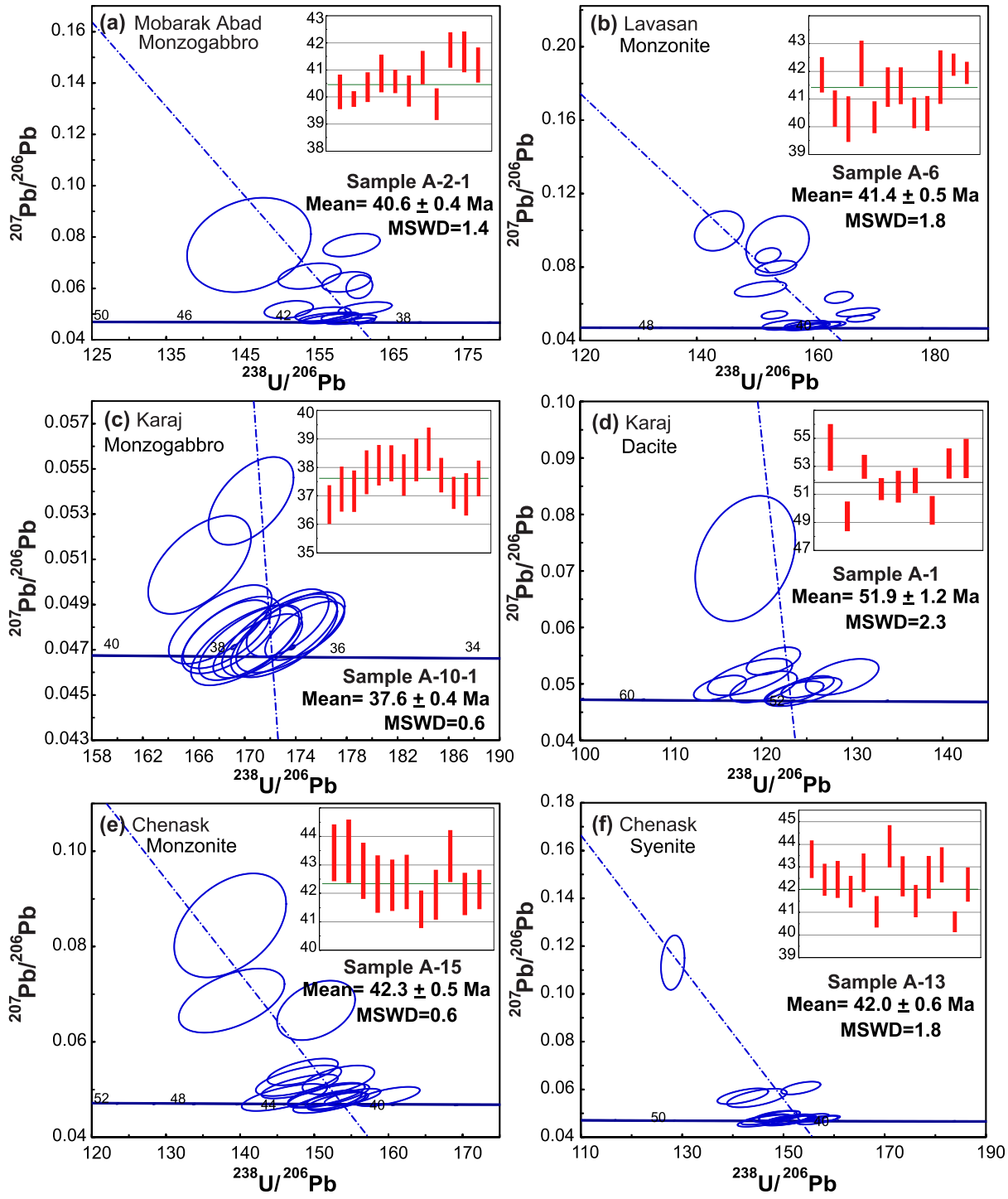

Fig. 8. U-Pb inverse-concordia ($^{207}Pb/^{206}Pb$ *vs* $^{238}U/^{206}Pb$) and weighted mean $^{206}Pb/^{238}U$ ages for zircons from the N Iran RA magmatic rocks.

6.1. Source of the N Iran igneous rocks

The N Iran RA igneous rocks consist of mafic to felsic lavas, with variable SiO_2 (49.2–72 wt%) and MgO (0.5–6.3 wt%) contents. They are mostly calc-alkaline to shoshonitic and show geochemical characteristics similar to normal I-type arc-related igneous rocks (Fig. 4). Both mafic and felsic intrusions have comparable rare-earth and trace elements patterns with similar isotopic values. Volcanic rocks are also similar in rare-earth and trace element patterns, but some seem isotopically to be more contaminated by country rocks; *e.g.* low bulk rock εNd and variable zircon εHf values. Bulk rock Sr-Nd isotope modelling confirm ~20% contamination of the volcanic rocks with the Neoproterozoic continental crust of Iran (Fig. 6A). Crustal contamination is also confirmed by abundant inherited zircons within the volcanic sample we dated. Geochemically, lavas are also similar to the intrusive rocks in terms of rare-earth and trace element patterns. These similarities, along with presence of the mafic counterparts (with high zircon εHf and bulk rock εNd values) and also lavas with contamination signatures, suggest derivation of N Iran RA parental magmas *via* mantle melting, which evolved to more felsic compositions *via* coupled assimilation-fractional crystallization (AFC) and/or Melting-Assimilation-Storage and Homogenization (MASH) processes. Negative correlation of Dy/Yb

ratios with increasing SiO_2 content (Fig. 9A) may reflect amphibole (± clinopyroxene) fractionation (Davidson et al., 2007). The CaO/Al_2O_3 *vs* FeO_{tot}/MgO plot (Fig. 9B) confirms amphibole (±clinopyroxene) fractionation, but also suggests that olivine and plagioclase probably fractionated during magma differentiation.

Arc-related signatures for N Iran RA intrusions and volcanic rocks include depletion in Nb-Ta and enrichment in both LILEs (*e.g.*, Cs, Rb, Th, U, and K) and LREEs (*e.g.*, La, Ce) (Pearce and Peate, 1995). The contribution of subduction components to the genesis of N Iran RA magmas is inferred from their high Th/Yb ratios in a Th/Yb *vs* Ta/Yb diagram (Fig. 9C). However, high Th/Yb ratio can also result from the interaction of ascending magmas with continental crust through AFC processes. The role of AFC processes on the N Iran RA rocks can be deduced from a Th/Yb *vs* SiO_2 plot (Fig. 9D). In this diagram, the more fractionated samples with high SiO_2 contents are characterized by higher Th/Yb ratios, confirming that some igneous rocks (especially volcanic rocks) assimilated more continental crust. This means that we must focus on mafic rocks to identify the mantle signature. High content of Ba and other large ion lithophile elements and low Nb abundance in these rocks (Ba/La = 5.4–39.1 and Nb/La = 0.2–1.1) ratios, are a conspicuous arc-related characteristics of N Iran RA igneous rocks, although these elements can also be influenced by the crustal contamination which is best recorded in the felsic rocks.

The trace elements (*e.g.*, high content of incompatible elements such as Nb-La) and isotopic (high zircon εHf- bulk rock εNd) geochemical signatures of the mafic precursors, which are less influenced by AFC processes, imply that RA parental melts were probably sourced from a mantle that was metasomatized by melts or fluids released from subducted altered oceanic crust (AOC) and/or sediments (Gertisser and Keller, 2003). The metasomatized mantle source for Iran RA

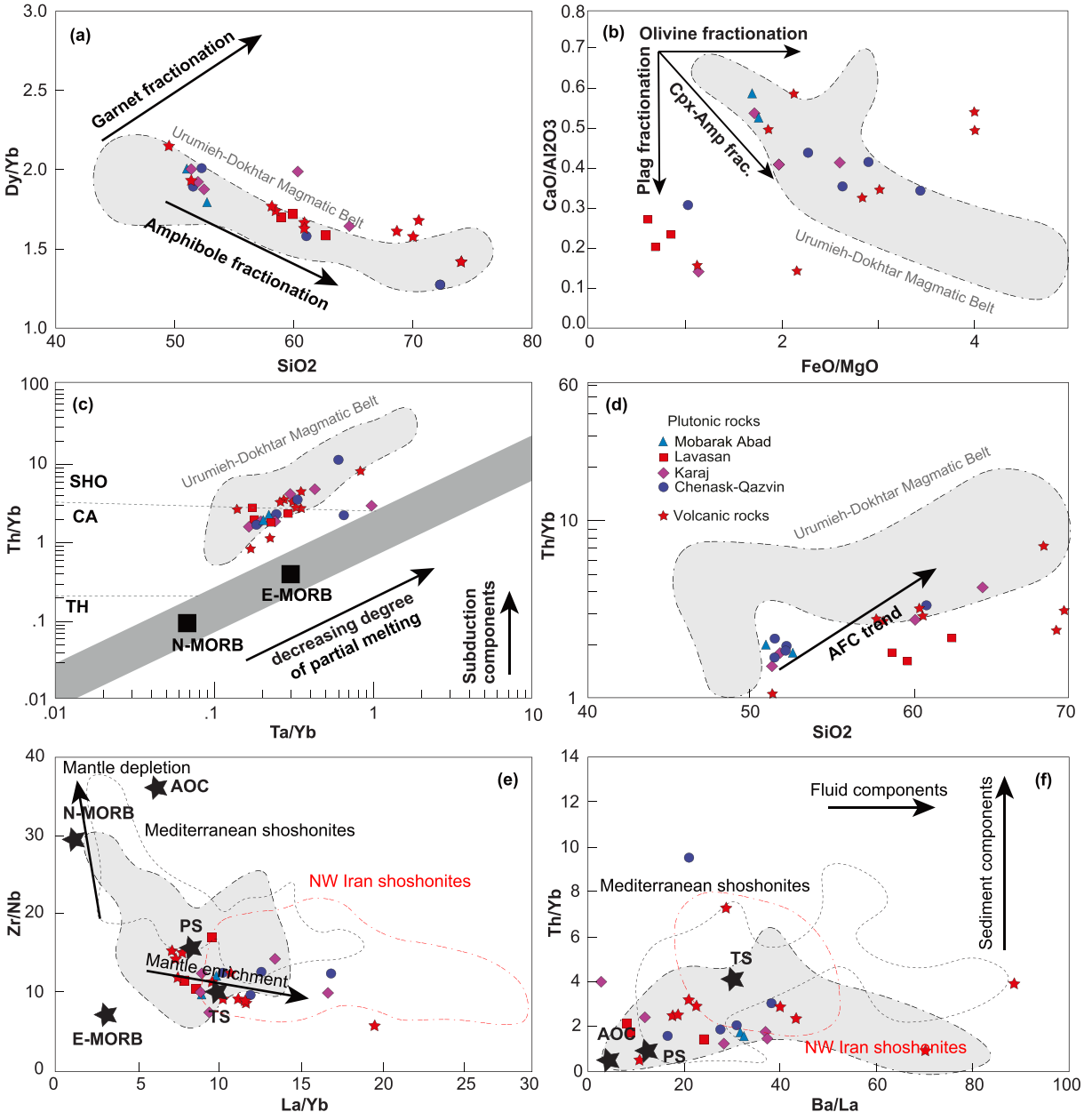

Fig. 9. Dy/Yb *vs* SiO_2 (a), CaO/Al_2O_3 *vs* FeO/MgO (b), Th/Yb *vs* Ta/Yb (c) and Th/Yb *vs* SiO_2 (d) diagrams for the N Iran RA rocks to track the FC and AFC processes during the genesis of these rocks. Zr/Nb *vs* La/Yb (e), and Th/Yb *vs* Ba/La (f) plots for tracing the mantle source of the N Iran RA rocks (modified after (Kirchenbaur and Münker, 2015)). The fields for Mediterranean shoshonites and Eastern Mediterranean sediments (EMS) are after (Kirchenbaur and Münker, 2015). The composition of altered oceanic crust (AOC), terrestrial (TS) and pelagic sediments (PS) are from (Todd et al., 2011). The composition of NW Iran shoshonites is from (Shafaii Moghadam et al., 2018). Data on Urumieh-Dokhtar Magmatic Belt (UDMB) are from (Honarmand et al., 2013) and Moghadam et al., (*unpublished data*).

magmatism was likely sub-continental lithospheric mantle (SCLM). Such a mantle source could also help explain the high-K content of the rear-arc magmatic rocks, a scenario that has also been proposed by (Asiabanha and Foden, 2012; Castro et al., 2013) for the genesis of high-K magmatic rocks in N and NW Iran. SCLM can also play a major role for the genesis of high-K rocks in the UDMB MF. Moreover, arc-related, high-alumina magmatic rocks generally have higher Th/Ce, Nb/Zr and Th/Nb ratios but low Pb/Nd than depleted MORB-sourced rocks. These geochemical characteristics are commonly interpreted to be the result of subducted sediment inputs into the mantle source (Gertisser and Keller, 2003). Intermediate to mafic igneous rocks from the N Iran RA show variably high Al_2O_3 contents (16.6–21.5 wt%) but variably low Th/Ce (0.03–0.12) and Th/Nb (0.14–0.59) ratios, implying that sediments had little effect on the magma source of these rocks. In contrast, in a Ba/La *vs* Th/Yb plot (Fig. 9F), it looks like subduction-related fluid components contributed more to the mantle source of N Iran RA magmas. However, felsic rocks with high Th/Yb and Ba/La ratios also indicate higher contribution of upper crust materials through AFC processes during their genesis. Low Zr/Nb but high La/Yb ratios of N Iran RA igneous rocks (Fig. 9E) imply that the mantle source was enriched, resembling that of NW Iran shoshonites (Moghadam et al., 2018).

6.2. Lu-Hf isotopic compositions of N Iran RA rocks

New zircon U-Pb ages show that volcanic rocks from the N Iran rear-arc began erupting by ~52 Ma and were intruded by younger gabbroic to granitic bodies (~38–42 Ma); these intrusions may mark the necks of eroded volcanoes. Zircons from monzogabbros have high εHf(t) values (+4.2 to +9.8), whereas monzonite zircons have slightly lower εHf (t) values (+1.8 to +8.7). Syenites also have moderately high εHf (t) values (+3 and + 7). The volcanic sample has zircons with variable εHf (t) values (+2.6 and − 9.2), indicating AFC processes had a major role during the genesis of these rocks. This is also confirmed by their low bulk rock εNd(t) values and the results of Sr-Nd isotope modelling (Fig. 6A).

The wide range of Hf isotopic composition of the N Iran RA plutonic (εHf = +1.8 to +9.8) and volcanic (εHf = −9.2 to +2.6) rocks precludes the simple evolution of these magmas by fractional crystallization, but other mechanisms such as wall-rock assimilation can explain the observed Hf isotope variations. This isotopic evolution suggests that early magmas interacted more with continental crust than later magmas. In a $^{176}Hf/^{177}Hf$ *vs* U-Pb age plot (Fig. 10A), it seems that AFC processes were important during the first stages (~8 Myr) of high-flux magmatism in N Iran (56–48 Ma), whereas juvenile magmas became increasingly important in the late Eocene (38–35 Ma). This is also confirmed by a $^{176}Hf/^{177}Hf$ *vs* SiO_2 plot (Fig. 10B) showing that fractionated rocks have lower and more variable $^{176}Hf/^{177}Hf$ values. This evolution suggests that conduits through the crust became better organized so that mantle-derived magma interacted less with continental crust with time. Mixed contributions from mantle and crustal sources are also indicated from isotopic compositions of ~ 42–60 Ma "flare-up" igneous rocks in the UDMB, when Hf isotopic compositions varied more (see next section). In summary, the heterogeneous distribution of zircon Hf-isotope data as well as whole-rock Nd isotopic compositions of N Iran RA rocks indicate that two discrete components, mantle-derived magmas and pre-existing continental crust or sediments, were involved in their genesis. The mantle source of mafic magmas was enriched, similar to SCLM, as shown in the zircon εHf(t) *vs* bulk rock εNd(t) plot (Fig. 6B). Partial melting of the SCLM has been similarly proposed for the genesis of high-K and shoshonitic magmas in both NW Iran and Anatolia (Aghazadeh et al., 2011; Castro et al., 2013).

6.3. Ages of rear arc vs magmatic front igneous rocks

To better understand the age variations along the UDMB and to understand its relationship to magmatic flare-up in the Iran arc, we compiled all Paleogene-Neogene age data from both MF and RA (regions 1 to 7 in Fig. 11A). We infer but do not know that there is a simple relationship between the number of dated samples and the volume of magma produced for that time. If this assumption is correct, then the age peaks shown in Fig. 11B-D can be interpreted as approximating magma generation rates, from which magma flare-up intervals can be inferred.

On the basis of limited data, (Verdel et al., 2007) suggested a magmatic flare-up in the MF that lasted ~17 Myrs, from ~54 Ma until 37 Ma. Our compilations agree with this overall assessment but show that increased igneous activity during this interval occurred at different times in different parts of Iran. Moreover, in the central and SE parts of the UDMB (MF), the flare-up lasted from 40 to 30 Ma (late Eocene-early Oligocene) (Fig. 11B), although magmatism started by ~60 Ma (Paleocene). A younger magmatic flare-up also occurred between 20 and 10 Ma (Miocene), mostly along the southern UDMB (Chiu et al., 2013; Verdel et al., 2007). In Saghand, between the MF and RA, the magmatic flare-up began earlier, lasting for 10 Myr from 55 to 45 Ma (early-middle Eocene) (Fig. 11C). In the RA between 39° and 36° N, the magmatic flare-up appears to have occurred in two stages; at 45 to 40 Ma and 30 to 25 Ma (Oligocene) (Fig. 11D). The RA seems to have experienced a magmatic lull at 35–40 Ma, when the UDMB magmatic front underwent a flare-up (compare Figs. 11B and D). Our compilations in Fig. 11 indicate that the magmatic flare-up probably began earlier in the RA than in MF. We emphasize that our assessment of magmatic flare-ups only considers the number of radiometric ages, we have not determined volumes of igneous rocks per unit time. We note that the compiled data comes mostly from plutonic rocks and few volcanic rocks. The UDMB contains thick sequences of middle Paleocene-Eocene pyroclastic rocks and interlayered lavas, which are missing in radiometric datasets

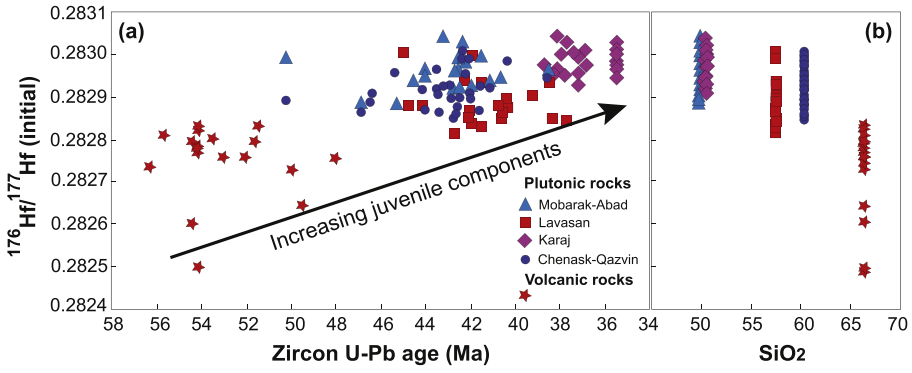

Fig. 10. $^{176}Hf/^{177}Hf$ (initial) *vs* zircon $^{206}Pb/^{238}U$ age (a) and SiO_2 (b). This shows that rear-arc magmas have less crustal influence with time and that felsic igneous rocks show the greatest crustal influence.

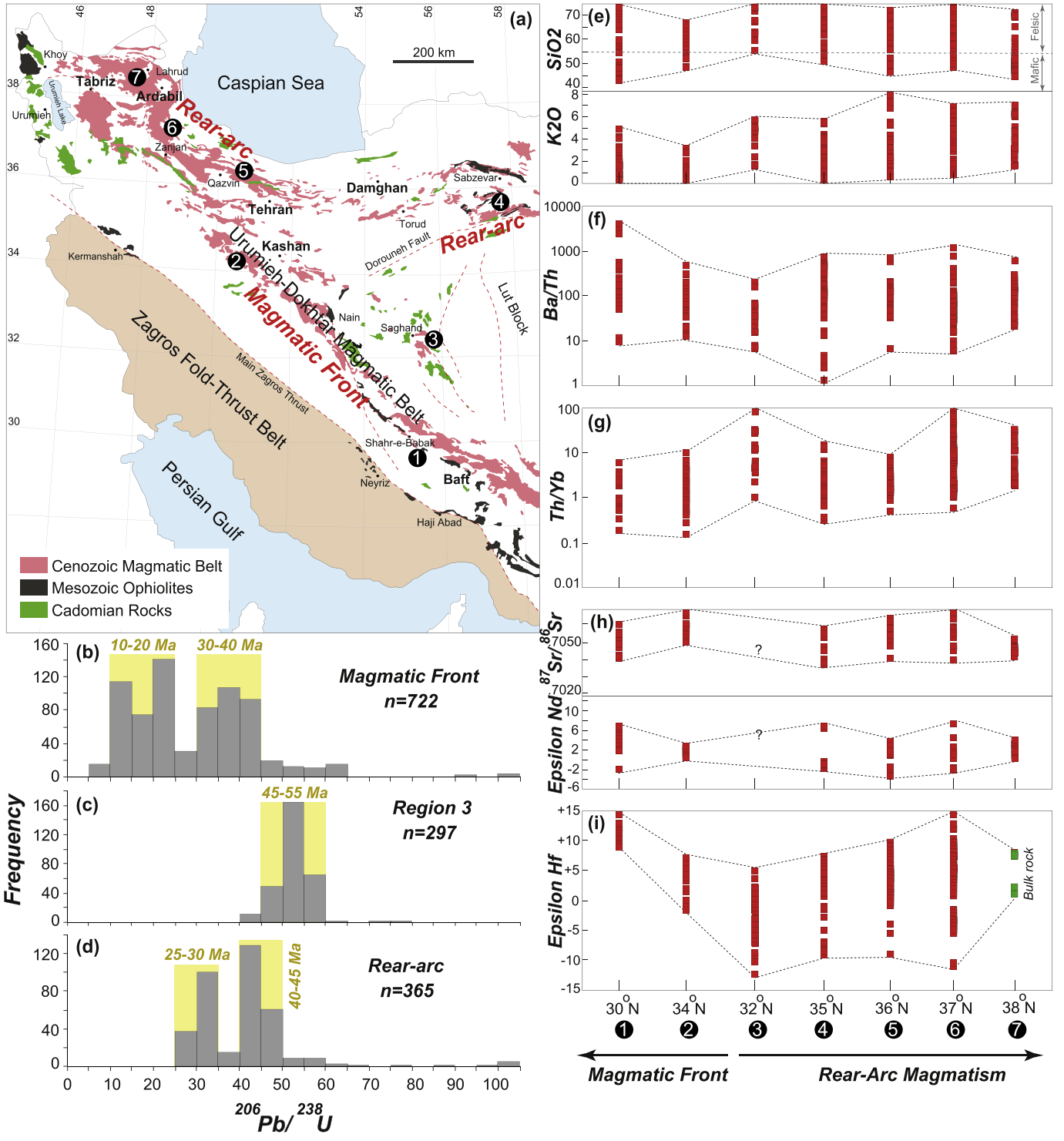

Fig. 11. Compiled data from both MF and RA regions of Iran arcs (a) to see the temporal variations of magmatism in MF and RA (b-d) and across-arc geochemical variations (e-i). Whole rock major-trace elements and isotope data for NW and N Iran magmatic rocks are from (Aghazadeh et al., 2011; Asiabanha and Foden, 2012; Castro et al., 2013) and (Moghadam et al., 2017). Data on Urumieh-Dokhtar Magmatic Belt (UDMB) and NE Iran are from (Honarmand et al., 2013; Moghadam et al., 2016; Sepidbar et al., 2018) and Moghadam et al., (*Unpublished data*). Zircon U-Pb-Hf isotope results on Iran arcs are from (Aghazadeh et al., 2011; Castro et al., 2013; Chiu et al., 2013; Chiu et al., 2017; Moghadam et al., 2016; Moghadam et al., 2017; Sepidbar et al., 2018) and Moghadam et al., (*unpublished data*).

due to lack of dated samples. The abundance of pyroclastic rocks (and interlayered lavas) confirm the explosive eruptions of Paleocene-early Eocene MF volcanoes, probably due to the high volatile contents of magmas characteristic of the arc magmatic front. Therefore, the magmatic flare-up started firstly at MF with explosive eruptions of pyroclastic materials and lavas. Afterwards, flare-up ignited the RA regions at ~45–40 Ma. In addition, the magmatic flare-up continued for a longer time, ~30 Myr (55–25 Ma), against the ~17 Myr suggested by (Verdel et al., 2007).

6.4. Across-arc geochemical variations

The origin of geochemical across-arc variations of arc igneous rocks continues to attract the attention of geoscientists. Across-arc variations

are well documented in many convergent margins where the subduction zone has a moderate slab dip angle. Igneous rocks associated with these convergent margins reveal a major shift in lava geochemistry between those from the magmatic front and those in the rear-arc (*e.g.*, Izu-Bonin, Kurile, Kamchatka, Central America, (Churikova et al., 2001; Hochstaedter et al., 2001)). The MF rocks have higher FeO/MgO ratio and are low-K tholeiites to calc-alkaline rocks, whereas RA magmatic rocks show medium- to low- FeO/MgO ratio and are high-K to shoshonitic lavas. For a given MgO content, RA magmatic rocks tend to have higher incompatible trace element concentrations than MF rocks. Elemental ratios involving both fluid-mobile and immobile elements and isotope ratios generally differ between MF and RA igneous rocks (Hochstaedter et al., 2001). The across-arc geochemical variations may be linked to the different factors such as (1) different degrees of partial melting beneath the MF and RA, perhaps caused by higher volatile fluxes from the subducted slab into the mantle wedge beneath the MF (Hochstaedter et al., 2001) and/or (2) differing source fertility due to the mantle wedge corner flow causing the transport of mantle materials that lost a melt component beneath the RA (Hochstaedter et al., 2001). The nature of released slab components depends on the thermal structure of the subducting oceanic slab and its depth in the subduction zone and thus the height of MF and RA magmatic centers above the subducted slab. For example, incompatible trace elements (LILE, HFSE; *e.g.*, Th, Rb, Pb, Nb) increase toward the RA region, perhaps due to a decrease in slab-related volatile input into the mantle wedge, which diminish the degrees of partial melting (Chiaradia et al., 2009). The lower degree of mantle melting beneath the RA would help explain the enrichment in incompatible elements in the RA magmatic rocks. Furthermore, ratios of fluid-mobile over immobile incompatible trace elements such as Ba/Th, Ba/Nb, Ba/La, Pb/Th, Pb/La increase toward the MF, suggesting greater slab dehydration and water flux below the MF (Ancellin et al., 2017). However, these elemental ratios strongly depend on the released slab components, which can vary from an aqueous-dominated fluid to hydrous silicate melt.

We used major and trace elements data as well as isotopes from Paleogene igneous rocks to draw the geochemical-isotopic across-arc trajectories from Iran MF to RA. Our compiled data show more felsic than mafic rocks in all of the Iran arc (11E). We must consider the role of the AFC in the genesis of felsic magmas, as shown by variations in incompatible trace element ratios and isotopic compositions. Although field observations suggest that the Iran RA has more mafic rocks (SiO_2 < 55%) compared to the MF which has more felsic igneous rocks (SiO_2 > 55%), our compilation suggests that the abundance of mafic and felsic rocks are similar in both MF and RA (Fig. 11). RA igneous rocks do tend to contain more K_2O than MF igneous rocks (Figs. 1 and 11) and high-K and shoshonitic rocks are restricted to the RA.

Ratios such as Ba/Th indicate an input of aqueous fluid into the mantle wedge source region because Ba is mobile in fluid or melt while Th is only mobile in silicate melts (Kessel et al., 2005). MF igneous rocks of the UDMB display higher Ba/Th ratios than those from the RA (*stdev.* = 92.4 ± 51), thus the subducted slab seems to dehydrate extensively beneath the MF, as seen for global arcs. However, some RA magmatic centers in NE Iran show variable Ba/Th ratios. Eocene RA igneous rocks from NE Iran with higher Ba/Th show adakitic-like signature (Moghadam et al., 2016). Th/Yb ratio also varies but generally increases toward the RA, especially at 36° to 38° N (N-NW Iran) (Fig. 11); this may indicate more sediment melt input, a role for garnet peridotite in RA melt generation, or some combination of these effects. RA igneous rocks at 32° N also have high Th/Yb ratios, but field relations show clear contamination with Neoproterozoic country rocks. Crustal contamination is also supported by fluctuations in zircon Hf isotope values.

Element partitioning between slab and fluids strongly influences the isotopic budget of hydrous fluids expelled from the slab. Pb and Sr are more mobile than Nd in these fluids (Kessel et al., 2005) and strongly affects the isotopic composition of the mantle source beneath the MF; in contrast Hf and Nd are liberated by sediment melting deeper in the subduction zone (Kelley et al., 2005). However, the influence of slab components (fluid *vs* melt) and the role of the continental crust must be considered for tracing isotope variability across the Iran convergent margin. Multistage partial melting of mantle wedge flowing from beneath the RA toward the MF will also provide more depleted mantle beneath the MF. For UDMB igneous rocks, the bulk rock εNd(t) and zircon εHf(t) values seem are highest in MF igneous rocks and across-arc isotopic variability seems to be mainly controlled by crustal influence. The highest $^{87}Sr/^{86}Sr$, lowest $^{143}Nd/^{144}Nd$ and most variable $^{176}Hf/^{177}Hf$ isotopic ratios are found in the RA (*e.g.*, region 6) where magmas were more contaminated by Neoproterozoic continental crust (Fig. 11).

6.5. Assimilation and fractional crystallization processes and zircon Lu-Hf isotope systematics

In this section, we discuss the significance of fractional crystallization (FC) and Assimilation-Fractional Crystallization (AFC) processes for Iran arc magmagenesis using major and trace element concentrations and Lu-Hf isotope variations in our new and compiled data from the MF and RA regions. Understanding the FC and AFC processes that controlled Iran arc magma evolution is important because it can help reconstruct how magma evolution and mineralization occurred across the Paleogene Iran convergent margin.

Our geochemical dataset (both our and compiled data) shows that both MF and RA magmatic rocks were affected by FC and AFC. These processes complicate identifying the mantle source signatures of MF and RA magmas. To better understand the role of the FC processes during the genesis of the MF and RA rocks, we plot our compiled data in a Mg# *vs* Ni diagram (Fig. 12). This diagram shows our dataset (n = 335 samples) includes more fractionated rocks (with Mg# <50) than nearly primitive ones with Mg# > 50% (66.6% fractionated *vs* 33.4% for near primitive rocks; considering primitive magmas with Mg# = 65, this value changes to ~ < 7% for primitive rocks). Magmas from NE (region 4 in Fig. 11), and NW (region 7) are more mafic, whereas most felsic rocks come from N Iran (region 5). We also plotted Ba/La, Nb/La, Sr/Nd and Pb/Ce ratios *vs* Mg# for Iran MF and RA rocks (Fig. 13). These trace element ratios overlap for both MF and RA rocks. More fractionated rocks with Mg# < 50 show a slight decrease in Sr/Nd ratio, which probably are related to the plagioclase fractionation. Both fractionated and primitive shoshonitic-adakitic rocks have lower Nb/La and Pb/Ce ratios, but higher Ba/La and Sr/Nd. These variations for the

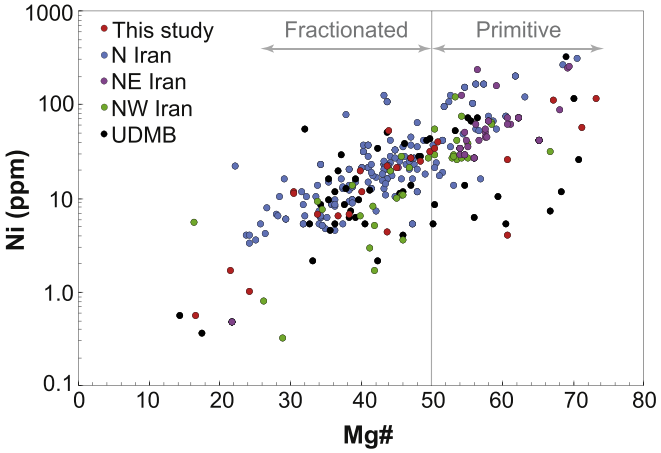

Fig. 12. Ni *vs* Mg# (100 Mg/Mg + Fe) plot for the compiled data from Iran MF and RA to evaluate the effects of fractional crystallization in our data. Data for NW and N Iran magmatic rocks are from (Aghazadeh et al., 2011; Asiabanha and Foden, 2012; Castro et al., 2013) and (Moghadam et al., 2017). Data on Urumieh-Dokhtar Magmatic Belt (UDMB) and NE Iran are from (Honarmand et al., 2013; Moghadam et al., 2016; Sepidbar et al., 2018) and Moghadam et al., (*unpublished data*).

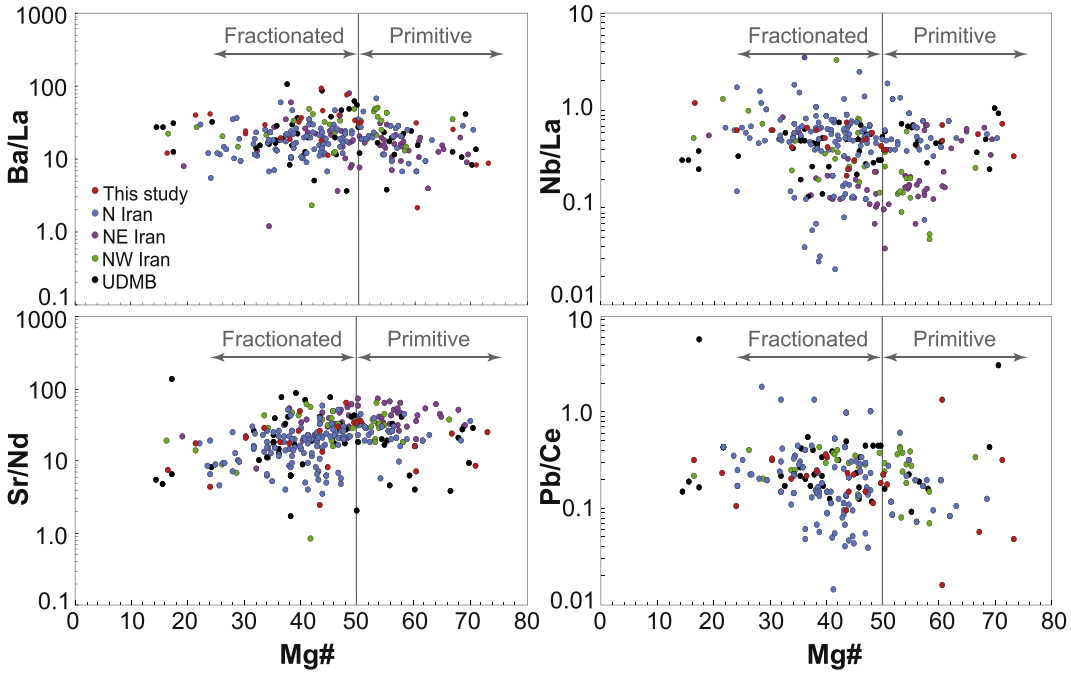

Fig. 13. Ba/La, Nb/La, Sr/Nd and Pb/Ce *vs* Mg# plots to track the relations between fractionation crystallization and variations of the trace elements ratios through MF to RA. Data for NW and N Iran magmatic rocks are from (Aghazadeh et al., 2011; Asiabanha and Foden, 2012; Castro et al., 2013) and (Moghadam et al., 2017). Data on Urumieh-Dokhtar Magmatic Belt (UDMB) and NE Iran are from (Honarmand et al., 2013; Moghadam et al., 2016; Sepidbar et al., 2018) and Moghadam et al., (*unpublished data*).

shoshonitic and adakitic rocks show compositional enrichment of their mantle source(s) and are not controlled by FC.

Zircon is a robust mineral for tracking the long-term magmatic evolution including the AFC processes (Andersen et al., 2004; Hawkesworth and Kemp, 2006). Regardless of the coexisting minerals, zircon has a very low Lu/Hf ratio ~0.005 and high Hf contents, which makes it useful as a Hf isotopic tracer. Both depleted mantle (T_{DM}) and crustal model ages (T^{C}_{DM}) are also considered to be useful for unravelling both the minimum source age of host magmas and the protolith crustal residence time, respectively. We calculated T_{DM} based on a mantle source similar to the depleted MORB mantle (DMM) with present-day $^{176}Hf/^{177}Hf = 0.28328$ (Salters and Stracke, 2004) and $^{176}Lu/^{177}Hf = 0.0384$ (Griffin et al., 2000), whereas T^{C}_{DM} was estimated by projecting the initial values of $^{176}Hf/^{177}Hf$ of a zircon to the depleted mantle growth curve, considering a $^{176}Lu/^{177}Hf$ value of 0.015 (Griffin et al., 2002). The compiled Hf isotope values and source model ages for all UDMB MF and RA Cenozoic rocks are presented in Figs. 14A and B.

The Hf isotopic compositions of different Cenozoic magmatic pulses (64–2 Ma) span an overall εHf(t) range of −43.2 to +19 ($^{176}Hf/^{177}Hf =$ 0.281521–0283283). Late Oligocene-Pliocene zircons exhibit more juvenile character (+14.9 to −16.4; *av* + 8.2) whereas Paleocene-early Oligocene zircons have a very wide range (+19 to −43.2; *av* + 2.2) (Fig. 14). Again, AFC processes seem to be more important during the first stages of Iran arc magmatism (66–27 Ma; Paleocene-early Oligocene), whereas more juvenile magmas became increasingly important in the late Oligocene-Pliocene (25–2 Ma) (Fig. 14B). Geographically, the magmas from SE UDMB (area 1 in Fig. 11, MF) and NE Iran (area 4 in Fig. 11, RA) are more juvenile than other parts of Iran arcs.

The calculated crustal Hf model ages (T^{C}_{DM}) for late Paleocene-early Oligocene (66–27 Ma) zircons with the least radiogenic Hf isotopic compositions vary between ~0.6 to 3.8 Ga (Fig. 14) and correspond to a difference of ~3.2 Ga in source crustal residence time, which reflect a possible heterogeneity of the underlying crust in different parts of the Cenozoic Iran arcs. Less radiogenic zircons from late Oligocene-Pliocene (25–2 Ma) rocks have T^{C}_{DM} values of 0.6–3 Ga. These values suggest involvement of Proterozoic to Archean crust for the formation of these rocks, although crust older than Ediacaran is unknown in Iran.

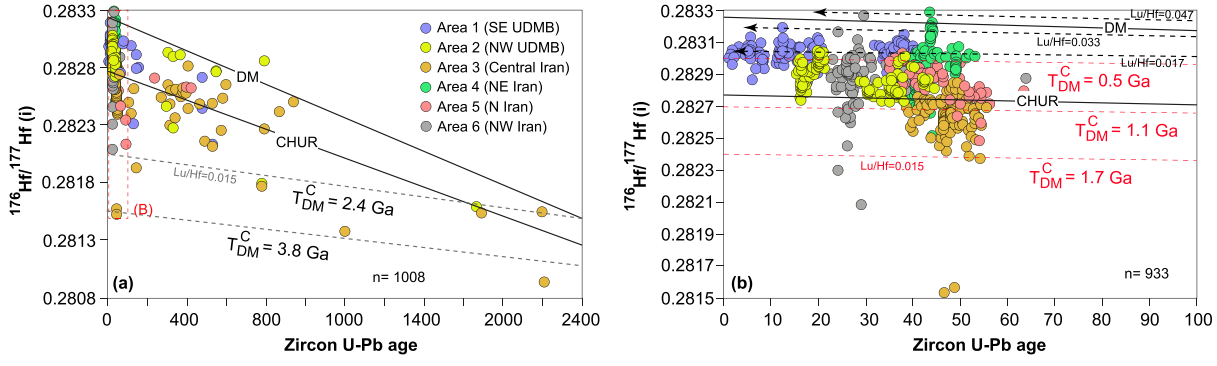

Fig. 14. Initial Hf isotopic composition of the magmatic (and inherited in "a") zircons from the Iranian arcs (areas 1 to 6 in Fig. 11) *vs* $^{206}Pb/^{238}U$ age of crystallization. The calculated crustal model ages (T^{C}_{DM}) relate to the $^{176}Lu/^{177}Hf$ ratio of 0.015; for a garnet-free crust. The $^{176}Lu/^{177}Hf$ ratios of 0.047, 0.033 and 0.017 are related to the required variations in the single (melting of isotopically heterogeneous reservoirs) and two component (interaction between mantle melts and upper crust materials) models that are crucial to explain the Cenozoic Lu-Hf isotope systematics. Zircon Lu-Hf isotope results on Iran arcs are from (Chiu et al., 2017; Moghadam et al., 2017; Sepidbar et al., 2018) and Moghadam et al., (*unpublished data*).

Two isotopic models have been advocated to be responsible for replicating the observed isotopic variations of Iran Cenozoic arc magmatic rocks (Andersen et al., 2007; Miskovic and Schaltegger, 2009). The first scenario simulates melting of isotopically heterogeneous reservoirs (*e.g.*, either a sub-continental lithospheric mantle or a juvenile lower continental crust) with nearly uniform T_{DM} ages (<0.6 Ga), with little or no continental crust contamination. This model explains isotopic arrays with restricted $^{176}Hf/^{177}Hf$ values, such as more radiogenic zircons ($\varepsilon Hf(t) > +7$) of Cenozoic age. For this single component model, the upper mantle (or juvenile lower crust) reservoirs could have evolved along both low and high $^{176}Lu/^{177}Hf$ ratios of 0.017 and 0.033 respectively since separating from the sources at ~0.5 Ga (Fig. 14B). Some zircons show evidence of evolving along a higher $^{176}Lu/^{177}Hf$ ratio of 0.047. The $^{176}Lu/^{177}Hf$ evolutionary trend of 0.017 is well within the average values of a magma reservoir which is barren of garnet, whereas the higher values of 0.033 to 0.047 shows the presence of an enriched reservoir probably containing garnet (with $^{176}Lu/^{177}Hf > 0.03$) (Miskovic and Schaltegger, 2009; Scherer et al., 2007). The presence of garnet in the source of such rocks is corroborated by their whole rocks steep HREE-MREE patterns.

On the other hand, the generation of Cenozoic magmas containing zircons with more variable but less radiogenic Hf isotopic ratios can be simulated using a two-component model, with mixing between a depleted mantle melt (with present-day $^{176}Hf/^{177}Hf = 0.28328$ (Salters and Stracke, 2004), $^{176}Lu/^{177}Hf = 0.0384$ (Griffin et al., 2000) and Hf = 2.31 ppm (Kelemen et al., 2003) and upper crustal materials (with present-day $^{176}Hf/^{177}Hf = 0.28242$ and $^{176}Lu/^{177}Hf = 0.0008$ and Hf = 5.12 ppm for upper crust (Gao et al., 1998)). To obtain the total range of $^{176}Hf/^{177}Hf$ observed in the Cenozoic zircons with more variable zircon Hf isotopic compositions, minor contamination with upper crustal materials (>5–25 mass % as computed using the formulation of (Miskovic and Schaltegger, 2009)) is needed over the time etween 0.6 to 3.8 Ga. The modelled upper crust contamination rate, using the Hf isotope variations within the UDMB (>5–25 mass %) is consistent with the bulk rock Sr-Nd modelling (Fig. 6A), which shows the UDMB rocks may have formed *via* contamination with 5 to ~20 mass % of Neoproterozoic upper crust or ~50% contamination by Neoproterozoic lower crust.

6.6. Hyperextension and arc magmatism in Iran

The Cenozoic Iran arc was similar in some ways to an Andean-type convergent margin, whereby subduction of oceanic crust triggered mantle melting, the melts of which interacted with the continental crust to generate both MF and RA (Fig. 15). However, the Cenozoic Iran arc differs significantly from the Andean continental arc, which reflects a convergent margin under compression, the crust of which is shortened and thickened. In contrast, the Iranian arc experienced strong extension throughout its evolution. Much of this extension accompanied subduction initiation during the Late Cretaceous and younger extension may have resulted from Paleogene slab roll-back (Moghadam et al., 2018; Moghadam and Stern, 2011). Alternatively, the MF and RA magmatism are better described in retreating (compressional) arcs such as Andes, but the extensional arcs such as Iran is enigmatic. In retreating arcs, the wide and volume of magmatic rocks are noticeable in the MF and the RA magmatic belt is mostly restricted to the ~100–200 km far from the main arc (MF). In some subduction systems, the rear-arc magmatism is located faraway from trench. For example, the Cenozoic rear-arc magmatism in the Oligocene San Juan Volcanic Field (US) erupted about 1000 km away from trench (Lake and Farmer, 2015). In recent extensional arcs such as Izu-Bonin-Mariana arc, the magmatic rocks are noticeable in RA, but are restricted to the 150–200 km far from the magmatic front (Kodaira et al., 2010). The distance of the RA from the main arc (MF) is a parameter than is controlled mainly by the dip of the subducting slab.

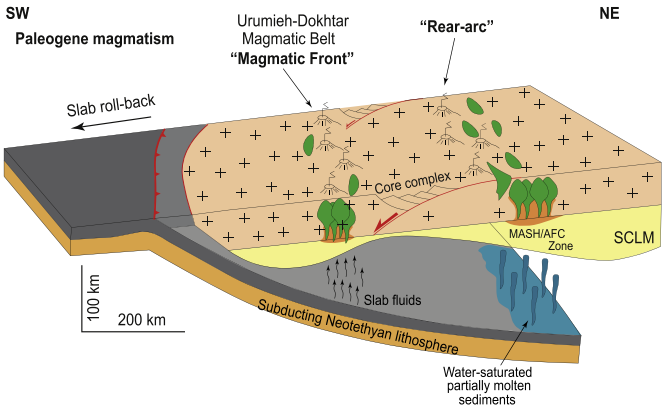

Fig. 15. Simplified cross-section of the Paleogene subduction zone in Iran, showing positions of magmatic front (MF) and rear-arc (RA); slab fluids *vs* sediment melts in MF and RA, Subcontinental Lithospheric Mantle (SCLM) melting and assimilation/fractional crystallization (AFC) or Melting-Assimilation-Storage-Homogenization (MASH) processes.

The Paleogene Iran arc contrasts strongly with the Andes and thus represents a useful magmatic-tectonic contrast. The extension triggered both lithospheric and asthenospheric mantle upwelling, resulting in a different magmatic style. This is obvious in the N-NW Iran RA magmatic belt, where calc-alkaline, shoshonitic to ultrapotassic and even nepheline-sodalite-bearing alkaline rocks coexist (Ashrafi et al., 2018; Moghadam et al., 2018). Therefore, we propose the distance of the RA from the MF in the extensional arcs like as Iran, is extremely dependent of the dip of the subducting Neotethyan slab. The change in the slab dip from Late Cretaceous to present can also control the spatial occurrence of magmatic rocks. This phenomena in close association with other triggers such as rifting in the RA due to the extreme extension will control the extent of the magmatic rocks, which in some cases can generate gigantic magmatism compared to the MF.

To evaluate the magmatic greatness, we calculated the magma volume per year of both MF and RA from 55 to 25 Ma. Using the exposed area (km^2) for igneous rocks of MF and RA and approximating the thickness of each as 30 ± 10 km, the magmatic rate is estimated to be ~12,000 ± 4000 km^3/yr^{-1} during the ~30 Myr magmatism for RA and ~ 64,000 ± 11,000 $km^3/yr^{-1}$for MF.

Alternating transgressive-regressive cycles preserved in Paleogene extensional basins suggest that the Paleogene tectonic evolution of Iran was complex. Both compression and extension likely occurred and may have been controlled by the age and convergence rate of subducted Neotethyan lithosphere, seamount or plateau subduction, trench retreat and roll-back. Cenozoic extension may have been related to the steepening dip of the Neotethyan slab and trench roll-back. Numerical modelling indicates that long-term subduction is not steady state and shows periodic shallowing and steepening of slab dip (Kay and Coira, 2009). Slab rollback may have been especially important because this is routinely associated with extension, crustal thinning and juvenile crustal addition (Miskovic and Schaltegger, 2009). Slab rollback is the most important cause of upper plate extension and has produced elevated rates of magma generation in nearly all arcs worldwide (Ducea et al., 2017). The effects of these processes differed in different parts of Iran and probably are linked to variations in crustal thickness.

A crustal profile of the Cenozoic arc of Iran can be reconstructed by using Sr/Y elemental ratios for intermediate rocks (Chapman et al., 2015) and Ce/Y ratios for mafic rocks (Mantle and Collins, 2008). (Chapman et al., 2015) suggested that Sr/Y ratios of intermediate calc-alkaline rocks (55–68 wt% SiO_2) can be used as a proxy for crustal thickness. Our compiled data for the intermediate SiO_2 composition of the Paleogene rocks show that the crustal thickness or Moho depth varied in different segments of Iran arcs; *av.* 42 km in N Iran (Alborz), 47–48 km in NE Iran and 27–28 km for the UDMB. These Moho depth results are confirmed by the Ce/Y ratio of the mafic rocks. These crustal

thickness variations show that lithospheric extension was more important for the MF (UDMB).

Eocene crustal thinning in the UDMB could also have been accompanied by lithospheric drips or delamination (*e.g.*, Pang et al., 2013). The other alternatives to explain the causes for the extreme extension during the Paleogene are changing slab dip (Verdel et al., 2007) and slab break-off (Deevsalar et al., 2017). However, the long-lived nature of magmatic events in the Iran convergent margin and irregular but widespread patterns of magmatism during late Mesozoic to Paleogene are inconsistent with either drip or delamination-related magmatism or slab break-off. The slab-break off and asthenosphere upwelling is probably the main mechanism for the telescopic occurrence of fertile Miocene plutonic rocks in the SE segment of the UDMB, which are the main causes for the Cu-Au mineralization. This occurred after the Iran-Arabia collision at ~25 Ma (McQuarrie and van Hinsbergen, 2013). The other concerns invoking the driving mechanisms for flare-up is suggested to be change in the rate of plate convergence. In this scenario, the flux melting will generate high-volume magmatism, which should be closely related to high-flux of slab-derived hydrous fluids. High-flux of slab-derived fluids can be correlated with subduction velocity. Such positive correlations have been observed in some arcs (*e.g.*, Huang and Lundstrom, 2007), although numerous studies elsewhere, however, show magmatic flare-up coincident with low and/or decreasing convergence rates (*e.g.*, Shellnutt et al., 2014) or no obvious correlation (Ducea et al., 2015; Zhang et al., 2019).

7. Conclusions

Iran arcs (both MF and RA) were generated during northward subduction of Neotethyan oceanic lithosphere accompanied by strong extension during Late Cretaceous and Paleogene time; extension stopped when collision with Arabia began at the beginning of Neogene time, ~25 Ma. Major and trace elements and bulk rock Sr-Nd- zircon Hf isotope analyses reveal an across-arc shift in the geochemical composition of Iran Paleogene arc magmas, from more depleted along the magmatic front to more enriched in the rear-arc. However, the across-arc geochemical shift is obscured by greater fractional crystallization and crustal contamination effects for rear-arc. Magmas which complicates understanding the underlying mantle sources and processes. Bulk rock εNd(t) and zircon εHf(t) isotope systematics show that melts of subcontinental lithospheric mantle interacted less with crust for the MF and more for the RA. The highest Th/Yb, $^{87}Sr/^{86}Sr$, but lowest $^{143}Nd/^{144}Nd$ and variable $^{176}Hf/^{177}Hf$ isotopic ratios are found in the RA where magmas seem to be highly contaminated with the Cadomian continental crust; variations in the composition of the mantle source are difficult to identify between MF abd RA.

Further research is needed to better understand magmagenesis beneath the Paleogene Iran convergent margin. A systematic geochemical-isotopic traverse across Iran arc is needed to better capture the across arc variation. This traverse should focus on sampling mafic igneous rocks because these are least affected by coupled fractional crystallization and crustal assimilation. Primitive (Mg# >65, Ni >100 ppm) basalts are especially useful in this effort because mantle melting processes are most easily reconstructed from these; in addition, melt inclusions in olivine can be analysed to determine magmatic fluid compositions.

Supplementary data to this article can be found online at https://doi.org/10.1016/j.lithos.2019.06.022.

Acknowledgments

We are very grateful to Iain Neill and an anonymous reviewer for their constructive reviews of the manuscript. Editorial suggestions by Xian-Hua Li are appreciated. This study was funded by the National Science Foundation of China (grant number 41703023). This is UTD Geosciences Dept. contribution # 1346. F. Sepidbar acknowledges support from the Iran Science Elites Federation. F.S. also thanks Y. Vesali for assistance during the field work.

References

Aghazadeh, M., Castro, A., Badrzadeh, Z., Vogt, K., 2011. Post-collisional polycyclic plutonism from the Zagros hinterland: the Shaivar Dagh plutonic complex, Alborz belt, Iran. Geol. Mag. 148, 980–1008.

Allen, M.B., Kheirkhah, M., Neill, I., Emami, M.H., Mcleod, C.L., 2013. Generation of Arc and Within-plate Chemical Signatures in Collision Zone Magmatism: Quaternary Lavas from Kurdistan Province, Iran. J. Petrol. 54, 887–911.

Ancellin, M.A., Samaniego, P., Vlastelic, I., Nauret, F., Gannoun, A., Hidalgo, S., 2017. Across-arc versus along-arc Sr-Nd-Pb isotope variations in the Ecuadorian volcanic arc. Geochem. Geophys. Geosyst. 18, 1163–1188.

Andersen, T., Griffin, W.L., Jackson, S.E., Knudsen, T.L., Pearson, N.J., 2004. Mid-Proterozoic magmatic arc evolution at the southwest margin of the Baltic Shield. Lithos 73, 289–318.

Andersen, T., Griffin, W.L., Sylvester, A.G., 2007. Sveconorwegian crustal underplating in southwestern Fennoscandia: LAM-ICPMS U-Pb and Lu-Hf isotope evidence from granites and gneisses in Telemark, southern Norway. Lithos 93, 273–287.

Ashrafi, N., Jahangiri, A., Hasebe, N., Eby, G.N., 2018. Petrology, geochemistry and geodynamic setting of Eocene-Oligocene alkaline intrusions from the Alborz-Azerbaijan magmatic belt, NW Iran. Geochemistry 78, 432–461.

Asiabanha, A., Foden, J., 2012. Post-collisional transition from an extensional volcano-sedimentary basin to a continental arc in the Alborz Ranges, N-Iran. Lithos 148, 98–111.

Ballato, P., Uba, C.E., Landgraf, A., Strecker, M.R., Sudo, M., Stockli, D.F., Friedrich, A., Tabatabaei, S.H., 2011. Arabia-Eurasia continental collision: Insights from late Tertiary foreland-basin evolution in the Alborz Mountains, northern Iran. Geol. Soc. Am. Bull. 123, 106–131.

Bell, K., Castorina, F., Lavecchia, G., Rosatelli, G., Stoppa, F., 2004. Is there a mantle plume below Italy? EOS Trans. Am. Geophys. Union 85, 541–547.

Belousova, E., Griffin, W.L., O'Reilly, S.Y., Fisher, N., 2002. Igneous zircon: trace element composition as an indicator of source rock type. Contrib. Mineral. Petrol. 143, 602–622.

Castillo, P.R., 2012. Adakite petrogenesis. Lithos 134–135, 304–316.

Castro, A., Aghazadeh, M., Badrzadeh, Z., Chichorro, M., 2013. Late Eocene-Oligocene post-collisional monzonitic intrusions from the Alborz magmatic belt, NW Iran. An example of monzonite magma generation from a metasomatized mantle source. Lithos 180, 109–127.

Chapman, J.B., Ducea, M.N., DeCelles, P.G., Profeta, L., 2015. Tracking changes in crustal thickness during orogenic evolution with Sr/Y: an example from the North American Cordillera. Geology 43, 919–922.

Chappell, B., 1999. Aluminium saturation in I-and S-type granites and the characterization of fractionated haplogranites. Lithos 46, 535–551.

Chauvel, C., Blichert-Toft, J., 2001. A hafnium isotope and trace element perspective on melting of the depleted mantle. Earth Planet. Sci. Lett. 190, 137–151.

Chiaradia, M., Merino, D., Spikings, R., 2009. Rapid transition to long-lived deep crustal magmatic maturation and the formation of giant porphyry-related mineralization (Yanacocha, Peru). Earth Planet. Sci. Lett. 288, 505–515.

Chiu, H.Y., Chung, S.L., Zarrinkoub, M.H., Mohammadi, S.S., Khatib, M.M., Iizuka, Y., 2013. Zircon U-Pb age constraints from Iran on the magmatic evolution related to Neotethyan subduction and Zagros orogeny. Lithos 162, 70–87.

Chiu, H.Y., Chung, S.L., Zarrinkoub, M.H., Melkonyan, R., Pang, K.N., Lee, H.Y., Wang, K.L., Mohammadi, S.S., Khatib, M.M., 2017. Zircon Hf isotopic constraints on magmatic and tectonic evolution in Iran: Implications for crustal growth in the Tethyan orogenic belt. J. Asian Earth Sci. 145, 652–669.

Churikova, T., Dorendorf, F., Worner, G., 2001. Sources and fluids in the mantle wedge below Kamchatka, evidence from across-arc geochemical variation. J. Petrol. 42, 1567–1593.

Davidson, J., MacPherson, C., Turner, S., 2007. Amphibole control in the differentiation of arc magmas. Geochim. Cosmochim. Acta 71, A204.

Deevsalar, R., Shinjo, R., Ghaderi, M., Murata, M., Hoskin, P.W.O., Oshiro, S., Wang, K.L., Lee, H.Y., Neill, I., 2017. Mesozoic-Cenozoic mafic magmatism in Sanandaj-Sirjan Zone, Zagros Orogen (Western Iran): Geochemical and isotopic inferences from Middle Jurassic and Late Eocene gabbros. Lithos 284, 588–607.

Defant, M.J., Drummond, M.S., 1990. Derivation of some modern arc magmas by melting of young subducted lithosphere. Nature 347, 662–665.

Ducea, M.N., Saleeby, J.B., Bergantz, G., 2015. The architecture, chemistry, and evolution of continental magmatic arcs. Annu. Rev. Earth Planet. Sci. 43 (43), 299–331.

Ducea, M.N., Bergantz, G.W., Crowley, J.L., Otamendi, J., 2017. Ultrafast magmatic buildup and diversification to produce continental crust during subduction. Geology 45, 235–238.

Ersoy, E.Y., Palmer, M.R., 2013. Eocene-Quaternary magmatic activity in the Aegean: Implications for mantle metasomatism and magma genesis in an evolving orogeny. Lithos 180, 5–24.

Etemad-Saeed, N., Hosseini-Barzi, M., Adabi, M.H., Miller, N.R., Sadeghi, A., Houshmandzadeh, A., Stockli, D.F., 2015. Evidence for ca. 560Ma Ediacaran Glaciation in the Kahar Formation, Central Alborz Mountains, Northern Iran. Gondwana Research.

Gao, S., Luo, T.C., Zhang, B.R., Zhang, H.F., Han, Y.W., Zhao, Z.D., Hu, Y.K., 1998. Chemical composition of the continental crust as revealed by studies in East China. Geochim. Cosmochim. Acta 62, 1959–1975.

Gertisser, R., Keller, J., 2003. Temporal variations in magma composition at Merapi Volcano (Central Java, Indonesia): magmatic cycles during the past 2000 years of explosive activity. J. Volcanol. Geotherm. Res. 123, 1–23.
Griffin, W.L., Pearson, N.J., Belousova, E., Jackson, S.E., van Achterbergh, E., O'Reilly, S.Y., Shee, S.R., 2000. The Hf isotope composition of cratonic mantle: LAM-MC-ICPMS analysis of zircon megacrysts in kimberlites. Geochim. Cosmochim. Acta 64, 133–147.
Griffin, W.L., Wang, X., Jackson, S.E., Pearson, N.J., O'Reilly, S.Y., Xu, X.S., Zhou, X.M., 2002. Zircon chemistry and magma mixing, SE China: In-situ analysis of Hf isotopes, Tonglu and Pingtan igneous complexes. Lithos 61, 237–269.
Griffin, W.L., Belousova, E.A., Shee, S.R., Pearson, N.J., O'Reilly, S.Y., 2004. Archean crustal evolution in the northern Yilgarn Craton: U-Pb and Hf-isotope evidence from detrital zircons. Precambrian Res. 131, 231–282.
Hart, S., Hauri, E., 1992. Mantle plumes and entrainment: isotopic evidence. Science 256, 517.
Hastie, A.R., Kerr, A.C., Pearce, J.A., Mitchell, S., 2007. Classification of altered volcanic island arc rocks using immobile trace elements: development of the Th–Co discrimination diagram. J. Petrol. 48, 2341–2357.
Hawkesworth, C.J., Kemp, A.I.S., 2006. Using hafnium and oxygen isotopes in zircons to unravel the record of crustal evolution. Chem. Geol. 226, 144–162.
Hochstaedter, A., Gill, J., Peters, R., Broughton, P., Holden, P., Taylor, B., 2001. Across-arc geochemical trends in the Izu-Bonin arc: Contributions from the subducting slab. Geochem. Geophys. Geosyst. 2.
Honarmand, M., Omran, N.R., Corfu, F., Emami, M.H., Nabatian, G., 2013. Geochronology and magmatic history of a calc-alkaline plutonic complex in the Urumieh-Dokhtar Magmatic Belt, Central Iran: zircon ages as evidence for two major plutonic episodes. Neues Jahrbuch Fur Mineralogie-Abhandlungen 190, 67–77.
Huang, F., Lundstrom, C.C., 2007. 231Pa excesses in arc volcanic rocks: Constraint on melting rates at convergent margins. Geology 35.
Jacques, G., Hoernle, K., Gill, J., Hauff, F., Wehrmann, H., Garbe-Schönberg, D., van den Bogaard, P., Bindeman, I., Lara, L.E., 2013. Across-arc geochemical variations in the Southern Volcanic Zone, Chile (34.5–38.0°S): Constraints on mantle wedge and slab input compositions. Geochim. Cosmochim. Acta 123, 218–243.
Jacques, G., Hoernle, K., Gill, J., Wehrmann, H., Bindeman, I., Lara, L.E., 2014. Geochemical variations in the Central Southern Volcanic Zone, Chile (38–43 S): the role of fluids in generating arc magmas. Chem. Geol. 371, 27–45.
Kargaranbafghi, F., Neubauer, F., Genser, J., 2015. Rapid Eocene extension in the Chapedony metamorphic core complex, Central Iran: Constraints from Ar-40/Ar-39 dating. J. Asian Earth Sci. 106, 156–168.
Kay, S.M., Coira, B.L., 2009. Shallowing and steepening subduction zones, continental lithospheric loss, magmatism, and crustal flow under the Central Andean Altiplano-Puna Plateau. Backbone of the Americas: Shallow Subduction, Plateau Uplift, and Ridge and Terrane Collision. 204, pp. 229–259.
Kelemen, P., Yogodzinski, G., Scholl, D., 2003. Along-strike variation in lavas of the Aleutian island arc: Implications for the genesis of high Mg# andesite and the continental crust. Inside the Subduction Factory, Geophysical Monograph. 138, pp. 223–276.
Kelley, K.A., Plank, T., Farr, L., Ludden, J., Staudigel, H., 2005. Subduction cycling of U, Th, and Pb. Earth Planet. Sci. Lett. 234, 369–383.
Kessel, R., Schmidt, M.W., Ulmer, P., Pettke, T., 2005. Trace element signature of subduction-zone fluids, melts and supercritical liquids at 120-180 km depth. Nature 437, 724–727.
Kirchenbaur, M., Münker, C., 2015. The behaviour of the extended HFSE group (Nb, Ta, Zr, Hf, W, Mo) during the petrogenesis of mafic K-rich lavas: the Eastern Mediterranean case. Geochim. Cosmochim. Acta 165, 178–199.
Kodaira, S., Noguchi, N., Takahashi, N., Ishizuka, O., Kaneda, Y., 2010. Evolution from fore-arc oceanic crust to island arc crust: a seismic study along the Izu-Bonin fore arc. J. Geophys. Res. 115.
Lake, E.T., Farmer, G.L., 2015. Oligo-Miocene mafic intrusions of the San Juan Volcanic Field, southwestern Colorado, and their relationship to voluminous, caldera-forming magmas. Geochim. Cosmochim. Acta 157, 86–108.
Lebas, M.J., Lemaitre, R.W., Streckeisen, A., Zanettin, B., 1986. A Chemical Classification of Volcanic-Rocks Based on the Total Alkali Silica Diagram. J. Petrol. 27, 745–750.
Mantle, G., Collins, W., 2008. Quantifying crustal thickness variations in evolving orogens: Correlation between arc basalt composition and Moho depth. Geology 36, 87–90.
McQuarrie, N., van Hinsbergen, D.J.J., 2013. Retrodeforming the Arabia-Eurasia collision zone: Age of collision versus magnitude of continental subduction. Geology 41, 315–318.
Middlemost, E.A., 1994. Naming materials in the magma/igneous rock system. Earth Sci. Rev. 37, 215–224.
Miller, K.G., Kominz, M.A., Browning, J.V., Wright, J.D., Mountain, G.S., Katz, M.E., Sugarman, P.J., Cramer, B.S., Christie-Blick, N., Pekar, S.F., 2005. The phanerozoic record of global sea-level change. Science 310, 1293–1298.
Miskovic, A., Schaltegger, U., 2009. Crustal growth along a non-collisional cratonic margin: a Lu-Hf isotopic survey of the Eastern Cordilleran granitoids of Peru. Earth Planet. Sci. Lett. 279, 303–315.
Moghadam, H.S., Stern, R.J., 2011. Geodynamic evolution of Upper cretaceous Zagros ophiolites: formation of oceanic lithosphere above a nascent subduction zone. Geol. Mag. 148, 762–801.
Moghadam, H.S., Khademi, M., Hu, Z.C., Stern, R.J., Santos, J.F., Wu, Y.B., 2015. Cadomian (Ediacaran-Cambrian) arc magmatism in the ChahJam-Biarjmand metamorphic complex (Iran): Magmatism along the northern active margin of Gondwana. Gondwana Res. 27, 439–452.
Moghadam, H.S., Rossetti, F., Lucci, F., Chiaradia, M., Gerdes, A., Martinez, M.L., Ghorbani, G., Nasrabady, M., 2016. The calc-alkaline and adakitic volcanism of the Sabzevar structural zone (NE Iran): Implications for the Eocene magmatic flare-up in Central Iran. Lithos 248, 517–535.
Moghadam, H.S., Griffin, W.L., Li, X.H., Santos, J.F., Karsli, O., Stern, R.J., Ghorbani, G., Gain, S., Murphy, R., O'Reilly, S.Y., 2017. Crustal evolution of NW Iran: cadomian arcs, archean fragments and the cenozoic magmatic flare-up. J. Petrol. 58, 2143–2190.
Moghadam, H.S., Griffin, W.L., Kirchenbaur, M., Garbe-Schnoberg, D., Khedr, M.Z., Kimura, J.I., Stern, R.J., Ghorbani, G., Murphy, R.C., O'Reilly, S.Y., 2018. Roll-back, extension and mantle upwelling triggered Eocene potassic magmatism in NW Iran. J. Petrol. 59, 1417–1465.
Neill, I., Meliksetian, K., Allen, M.B., Navarsardyan, G., Karapetyan, S., 2013. Pliocene-Quaternary volcanic rocks of NW Armenia: Magmatism and lithospheric dynamics within an active orogenic plateau. Lithos 180, 200–215.
Neill, I., Meliksetian, K., Allen, M.B., Navasardyan, G., Kuiper, K., 2015. Petrogenesis of mafic collision zone magmatism: the Armenian sector of the Turkish-Iranian Plateau. Chem. Geol. 403, 24–41.
Pang, K.N., Chung, S.L., Zarrinkoub, M.H., Khatib, M.M., Mohammadi, S.S., Chiu, H.Y., Chu, C.H., Lee, H.Y., Lo, C.H., 2013. Eocene-Oligocene post-collisional magmatism in the Lut-Sistan region, eastern Iran: Magma genesis and tectonic implications. Lithos 180, 234–251.
Pearce, J.A., Peate, D.W., 1995. Tectonic implications of the composition of volcanic arc magmas. Annu. Rev. Earth Planet. Sci. 23, 251–285.
Pearce, J., Kempton, P., Nowell, G., Noble, S., 1999. Hf-Nd element and isotope perspective on the nature and provenance of mantle and subduction components in Western Pacific arc-basin systems. J. Petrol. 40, 1579–1611.
Salters, V.J., Stracke, A., 2004. Composition of the depleted mantle. Geochem. Geophys. Geosyst. 5.
Schaltegger, U., Fanning, C.M., Günther, D., Maurin, J.C., Schulmann, K., Gebauer, D., 1999. Growth, annealing and recrystallization of zircon and preservation of monazite in high-grade metamorphism: conventional and in-situ U-Pb isotope, cathodoluminescence and microchemical evidence. Contrib. Mineral. Petrol. 134, 186–201.
Scherer, E.E., Whitehouse, M.J., Münker, C., 2007. Zircon as a monitor of crustal growth. Elements 3, 19–24.
Sepidbar, F., Mirnejad, H., Ma, C., Moghadam, H.S., 2018. Identification of Eocene-Oligocene magmatic pulses associated with flare-up in East Iran: timing and sources. Gondwana Res. 57, 141–156.
Shellnutt, J.G., Lee, T.Y., Brookfield, M.E., Chung, S.L., 2014. Correlation between magmatism of the Ladakh Batholith and plate convergence rates during the India-Eurasia collision. Gondwana Res. 26, 1051–1059.
Streckeisen, A., 1979. Classification of Volcanic-Rocks, Lamprophyres, Carbonatites, and Melilitic Rocks - Recommendations and Suggestions of the Iugs Subcommission on the Systematics of Igneous Rocks - Reply. Geology 7, 562.
Sun, S.-S., McDonough, W.-S., 1989. Chemical and isotopic systematics of oceanic basalts: implications for mantle composition and processes. Geol. Soc. Lond. Spec. Publ. 42, 313–345.
Todd, E., Gill, J.B., Wysoczanski, R.J., Hergt, J., Wright, I.C., Leybourne, M.I., Mortimer, N., 2011. Hf isotopic evidence for small-scale heterogeneity in the mode of mantle wedge enrichment: Southern Havre Trough and South Fiji Basin back arcs. Geochem. Geophys. Geosyst. 12.
Verdel, C., Wernicke, B.P., Ramezani, J., Hassanzadeh, J., Renne, P.R., Spell, T.L., 2007. Geology and thermochronology of Tertiary Cordilleran-style metamorphic core complexes in the Saghand region of central Iran. Geol. Soc. Am. Bull. 119, 961–977.
Verdel, C., Wernicke, B.P., Hassanzadeh, J., Guest, B., 2011. A Paleogene extensional arc flare-up in Iran. Tectonics 30.
Vervoort, J.D., Blichert-Toft, J., 1999. Evolution of the depleted mantle: Hf isotope evidence from juvenile rocks through time. Geochim. Cosmochim. Acta 63, 533–556.
Wang, B., Chen, J., Xu, J., Wang, L., 2014. Geochemical and Sr–Nd–Pb–Os isotopic compositions of Miocene ultrapotassic rocks in southern Tibet: Petrogenesis and implications for the regional tectonic history. Lithos 208, 237–250.
Wehrmann, H., Hoernle, K., Garbe-Schonberg, D., Jacques, G., Mahlke, J., Schumann, K., 2014. Insights from trace element geochemistry as to the roles of subduction zone geometry and subduction input on the chemistry of arc magmas. Int. J. Earth Sci. 103, 1929–1944.
Zhang, Z., Xiao, W., Ji, W., Majidifard, M.R., Rezaeian, M., Talebian, M., Xiang, D., Chen, L., Wan, B., Ao, S., Esmaeili, R., 2018. Geochemistry, zircon U-Pb and Hf isotope for granitoids, NW Sanandaj-Sirjan zone, Iran: Implications for Mesozoic-Cenozoic episodic magmatism during Neo-Tethyan lithospheric subduction. Gondwana Res. 62, 227–245.
Zhang, X., Chung, S.-L., Lai, Y.-M., Ghani, A.A., Murtadha, S., Lee, H.-Y., Hsu, C.-C., 2019. A 6000-km-long Neo-Tethyan arc system with coherent magmatic flare-ups and lulls in South Asia. Geology 47, 573–576.
Zindler, A., Hart, S., 1986. Chemical geodynamics. Annu. Rev. Earth Planet. Sci. 14, 493–571.